MHD-kinetic hybrid code based on structure-preserving finite elements with particles-in-cell

Florian Holderied[1,2,*], Stefan Possanner[1,3], and Xin Wang[1]

[1] *Max Planck Institute for Plasma Physics, Boltzmannstrasse 2, 85748 Garching, Germany*

[2] *Technical University of Munich, Department of Physics, James-Franck-Strasse 1, 85748 Garching, Germany*

[3] *Technical University of Munich, Department of Mathematics, Boltzmannstrasse 3, 85748 Garching, Germany*

[*] *Corresponding author: Florian Holderied, florian.holderied@ipp.mpg.de*

Abstract

We present a STRUcture-Preserving HYbrid code (STRUPHY) for the simulation of shear-Alfvén waves interacting with a small population of energetic particles far from thermal equilibrium (kinetic species). It features linearized magneto-hydrodynamic (MHD) equations, coupled nonlinearly to either full-orbit Vlasov equations via a current coupling scheme. The algorithm is based on finite element exterior calculus (FEEC) for the MHD part and particle-in-cell (PIC) methods for the kinetic part, implemented for arbitrary Riemannian metric in three space dimensions. Noise-reduction via a control variate is optional for the PIC part (δf in contrast to full-f). In the full-f version without control variate, STRUPHY is structure-preserving in the sense that it preserves the discrete mass, discrete energy, zero-divergence constraint and magnetic helicity up to machine precision, independent of metric and mesh parameters. Several numerical tests are presented that demonstrate this behavior.

1 Introduction

Plasma waves in magneto-hydrodynamic (MHD) fluids can be resonantly excited by energetic particles with thermal speeds in the range of the Alfvén velocity. Such wave-particle interactions are observed for instance in deuterium-tritium fusion reactors, where hot α-particles can destabilize shear Alfvén modes and thus compromise confinement time [19, 22, 11]. Another example is the interaction of energetic electrons in the solar wind with Whistler waves propagating in Earth's magnetosphere. This interaction can lead to new types of electromagnetic waves whose spectrograms show discrete elements with rising or falling frequencies with respect to time (also known as frequency chirping) [32, 9, 28]. The associated nonlinear dynamics in realistic scenarios such as fusion reactors or solar wind can be studied via computer simulation of suitable model equations. The latter range from full kinetic models of all involved plasma species (bulk and energetic particles), over hybrid codes to reduced fluid simulations, all compared in a recent benchmark study [20]. The notion of a "hybrid code" implies the following two crucial features:

1. Use of reduced model equations for bulk plasma (for instance fluid instead of kinetic).
2. Fully self-consistent description of nonlinear dynamics (beyond the linear phase).

Examples of successful implementations of hybrid codes are MEGA [30], M3D-K [5, 26], HMGC [6] and HMGC-X [33]. The appeal of hybrid codes is three-fold: a) reduced numerical cost compared to fully kinetic simulations, b) inclusion of non-equilibrium dynamics (wave-particle resonances) compared to pure fluid simulations and c) possibility of direct comparison with analytic computations (for linear dynamics). The drawback is the increased complexity of model equations. For instance, while the geometric structure (ie. Poisson bracket and/or variational principle) of MHD equations has been known for decades [25], the underlying structure of MHD-kinetic hybrid models has been discovered only very recently [31, 8]. This shows that the proper derivation of MHD-kinetic hybrids that respect fundamental physics principles such as energy conservation is a non-trivial task. As a consequence, little attention had been paid to these issues during the design of the first generation of hybrid codes mentioned above.

In parallel to the theoretical discoveries on how to construct proper hybrid models came the advent of geometric (or structure-preserving) methods for plasma equations, see [24] for a review. These obey many of the conservation properties implied by the geometric structure on the discrete level, such as energy, charge or momentum. The main idea is to discretize directly the underlying Poisson structure or variational principle, thus transferring geometric properties to a finite-dimensional setting. The very first structure-preserving geometric PIC algorithm was designed and implemented by Squire et al. in 2012 [29]. Similar methods have later been successfully applied to Vlasov-Maxwell [17, 27, 36, 35], Vlasov-Darwin [10] and Vlasov-Poisson equations [14, 34]. The first structure-preserving geometric PIC algorithm using finite element exterior calculus (FEEC) was designed by He et al. in 2016 [18]. The same approach has later been taken by Kraus et al. [21] who used B-spline basis functions to efficiently build the discrete deRham complex, which contains Nédélec and Raviart-Thomas spaces. The theoretical foundation of FEEC has been laid by Arnold et al. [3, 1]; the interested reader may consult the recent book of Arnold [2] for a comprehensive overview.

In this work we apply the ideas of structure-preserving integration to a MHD-kinetic hybrid model, namely the Hamiltonian current-coupling (CC) scheme [31] In the version of the code presented here, we linearize the MHD part and focus on the nonlinear coupling to the kinetic species, which acts back on the bulk plasma via charge and current densities (CC). FEEC is used for the discretization of the MHD part in three space dimensions and PIC for the kinetic part. We discretize the equations rather than the variational principle or the Poisson bracket, in order to avoid unnecessary abstraction. Moreover, the linearized MHD equations might lose their Hamiltonian structure if the magnetic background field is not chosen properly. In this case there is no such thing as a Poisson bracket or variational formulation, but our method of discretization still applies. In the semi-discrete setting with continuous time variable, we arrive at a non-canonical Hamiltonian system of ordinary differential equations with skew-symmetric Poisson matrix, which directly implies conservation of energy. The conservation of zero-divergence and helicity follow from the proper choice of FEEC spaces (Nédélec and Raviart-Thomas). The conservation laws are satisfied independent of the chosen metric and mesh parameters thanks to the separation between topological and metric properties in the theory of differential forms, upon which FEEC is built. We then use Poisson splitting and show that the described conservation laws translate to the fully discrete setting.

This article is organized as follows. Section 2 first introduces the basic model equations along with some of its properties on the continuous level, followed by a derivation of a coordinate-free representation of the model in terms of differential forms to prepare the application of FEEC. Based on this result, Section 3 describes in detail the spatial discretization of a proper weak formulation using FEEC, followed by a discussion of some properties of the resulting semi-discrete system of ordinary differential equations with continuous time variable. We also review the realization of the compatible finite element spaces along with projection operators on these spaces using B-spline basis functions, which are used in this work. Section 4 is devoted to the proposed time integration scheme based on Poisson splitting. Numerical results are shown in Section 5 before we summarize and conclude in Section 6. Additionally, this article contains two appendices. Appendix A contains formulae for the exterior calculus of differential forms including transformation formulae to vector and scalar fields, respectively. While we focus on the full-f method in the main text, Appendix B outlines the modifications that have to be made if the δf method is used.

2 Model equations

2.1 Hamiltonian current coupling

Our target model is a MHD-kinetic hybrid model in which the coupling between fluid bulk and kinetic species (subscript "h" for "hot") appears through the Lorentz force terms. This is called current-coupling (CC) and involves the first two moments of the kinetic species' distribution function f_{h}, namely the charge density $\rho_{\mathrm{ch}} = \rho_{\mathrm{h}}(t, \boldsymbol{x})$ and the current density $\boldsymbol{J}_{\mathrm{h}} = \boldsymbol{J}_{\mathrm{h}}(t, \boldsymbol{x})$. Denoting by $\nabla = (\partial_x, \partial_y, \partial_z)^\top$ and $\nabla_{\boldsymbol{v}} = (\partial_{v_x}, \partial_{v_y}, \partial_{v_z})^\top$ the nabla-operator acting on spatial and velocity coordinates, respectively, the Hamiltonian CC in SI-units reads

$$\text{MHD} \quad \begin{cases} \dfrac{\partial \rho}{\partial t} + \nabla \cdot (\rho \boldsymbol{U}) = 0, \\ \rho \left[\dfrac{\partial \boldsymbol{U}}{\partial t} + (\boldsymbol{U} \cdot \nabla) \boldsymbol{U} \right] = \rho_{\mathrm{h}} (\boldsymbol{U} \times \boldsymbol{B}) + \left(\dfrac{\nabla \times \boldsymbol{B}}{\mu_0} - \boldsymbol{J}_{\mathrm{h}} \right) \times \boldsymbol{B} - \nabla p, \\ \dfrac{\partial p}{\partial t} + \nabla \cdot (p \boldsymbol{U}) + (\gamma - 1) p \nabla \cdot \boldsymbol{U} = 0, \\ \dfrac{\partial \boldsymbol{B}}{\partial t} = \nabla \times (\boldsymbol{U} \times \boldsymbol{B}), \end{cases} \tag{2.1a}$$

$$\text{kinetics} \quad \begin{cases} \dfrac{\partial f_{\mathrm{h}}}{\partial t} + \boldsymbol{v} \cdot \nabla f_{\mathrm{h}} + \dfrac{q_{\mathrm{h}}}{m_{\mathrm{h}}} (\boldsymbol{B} \times \boldsymbol{U} + \boldsymbol{v} \times \boldsymbol{B}) \cdot \nabla_{\boldsymbol{v}} f_{\mathrm{h}} = 0, \\ \rho_{\mathrm{h}} = q_{\mathrm{h}} \displaystyle\int_{\mathbb{R}^3} f_{\mathrm{h}} \, \mathrm{d}^3 v, \qquad \boldsymbol{J}_{\mathrm{h}} = q_{\mathrm{h}} \displaystyle\int_{\mathbb{R}^3} \boldsymbol{v} f_{\mathrm{h}} \, \mathrm{d}^3 v, \end{cases} \tag{2.1b}$$

supplemented to the zero-divergence constraint $\nabla \cdot \boldsymbol{B} = 0$. This set of equations forms a closed system of nonlinear partial differential equations describing the evolution of the mass density $\rho = \rho(t, \boldsymbol{x})$, mean velocity $\boldsymbol{U} = \boldsymbol{U}(t, \boldsymbol{x})$, pressure $p = p(t, \boldsymbol{x})$, magnetic induction $\boldsymbol{B} = \boldsymbol{B}(t, \boldsymbol{x})$ (which we will simply refer to as magnetic field) hot ion distribution function $f_{\mathrm{h}} = f_{\mathrm{h}}(t, \boldsymbol{x}, \boldsymbol{v})$. The system is defined for times $t \in \mathbb{R}_0^+$ in a domain $\Omega \subset \mathbb{R}^3$ with smooth boundary $\partial\Omega$ and supplemented with suitable initial and boundary conditions. Furthermore, $\gamma = 5/3$ is the heat capacity ratio of an ideal gas and μ_0 denotes the vacuum permeability, q_{h} the kinetic species' charge[1] and m_{h} its mass. The model is based on common assumptions made in MHD:

1. Quasi-neutrality ($\rho_{\mathrm{c}} \to 0$),
2. Characteristic velocities well-below the speed of light ($|\boldsymbol{U}| \ll c$),
3. Negligence of electron inertia ($m_{\mathrm{e}} \to 0$),
4. Ohm's law of the form $\boldsymbol{E} = -\boldsymbol{U} \times \boldsymbol{B}$ (*ideal* MHD: plasma resistivity $\sigma \to 0$).

In the following we set μ_0, q_{h} and m_{h} to one for better readability.

The system (2.1) possesses a noncanonical Hamiltonian structure, i.e. in can be derived from a Poisson bracket together with the conserved Hamiltonian

$$\mathcal{H}_0(t) = \frac{1}{2} \int_\Omega \rho \boldsymbol{U}^2 \, \mathrm{d}^3 x + \frac{1}{\gamma - 1} \int_\Omega p \, \mathrm{d}^3 x + \frac{1}{2} \int_\Omega \boldsymbol{B}^2 \, \mathrm{d}^3 x + \frac{1}{2} \int_\Omega \int_{\mathbb{R}^3} \boldsymbol{v}^2 f_{\mathrm{h}} \, \mathrm{d}^3 v \, \mathrm{d}^3 x, \tag{2.2}$$

which is equal to the total energy of the system [31]. Other conserved quantities are the total mass, momentum and the magnetic helicity

$$M(t) = \int_\Omega \rho \, \mathrm{d}^3 x + \int_\Omega \int_{\mathbb{R}^3} f_{\mathrm{h}} \, \mathrm{d}^3 v \, \mathrm{d}^3 x, \tag{2.3}$$

$$\boldsymbol{P}(t) = \int_\Omega \rho \boldsymbol{U} \, \mathrm{d}^3 x + \int_\Omega \int_{\mathbb{R}^3} \boldsymbol{v} f_{\mathrm{h}} \, \mathrm{d}^3 v \, \mathrm{d}^3 x, \tag{2.4}$$

$$H_m(t) = \int_\Omega \boldsymbol{A} \cdot \boldsymbol{B} \, \mathrm{d}^3 x, \tag{2.5}$$

where $\boldsymbol{A}$ is the magnetic vector potential from which the magnetic field can be obtained via $\boldsymbol{B} = \nabla \times \boldsymbol{A}$.

[1] We assume hot ions with positive charge.

2.2 Linearization of the MHD part

In this work we shall consider CC with linearized MHD. This is sufficient for describing the three fundamental types of waves in ideal MHD, that are, the slow and fast magnetosonic wave and the shear Alfvén wave. Consequently, the present work cannot capture MHD turbulence, which will be the topic of future studies within this framework. Assuming that MHD waves are small perturbations (denoted by tildes) with respect to a pre-defined equilibrium state (denoted by the subscript "eq") satisfying $\nabla p_{\text{eq}} = (\nabla \times \boldsymbol{B}_{\text{eq}} - \boldsymbol{J}_{\text{h,eq}}) \times \boldsymbol{B}_{\text{eq}}$, we make the ansatzes $\rho = \rho_{\text{eq}} + \tilde{\rho}$, $\boldsymbol{U} = \tilde{\boldsymbol{U}}$ (zero-flow equilibrium), $p = p_{\text{eq}} + \tilde{p}$ and $\boldsymbol{B} = \boldsymbol{B}_{\text{eq}} + \tilde{\boldsymbol{B}}$ for the MHD variables, plug it in (2.1a) and neglect all nonlinear terms expect for the ones involving the kinetic particles. The partially linearized model then reads

$$\text{MHD} \quad \begin{cases} \dfrac{\partial \tilde{\rho}}{\partial t} + \nabla \cdot (\rho_{\text{eq}} \tilde{\boldsymbol{U}}) = 0, \\ \rho_{\text{eq}} \dfrac{\partial \tilde{\boldsymbol{U}}}{\partial t} = (\nabla \times \tilde{\boldsymbol{B}}) \times \boldsymbol{B}_{\text{eq}} + (\nabla \times \boldsymbol{B}_{\text{eq}}) \times \tilde{\boldsymbol{B}} + (\rho_{\text{h}} \tilde{\boldsymbol{U}} - \boldsymbol{J}_{\text{h}}) \times \boldsymbol{B} - \nabla \tilde{p}, \\ \dfrac{\partial \tilde{p}}{\partial t} + \nabla \cdot (p_{\text{eq}} \tilde{\boldsymbol{U}}) + (\gamma - 1) p_{\text{eq}} \nabla \cdot \tilde{\boldsymbol{U}} = 0, \\ \dfrac{\partial \tilde{\boldsymbol{B}}}{\partial t} = \nabla \times (\tilde{\boldsymbol{U}} \times \boldsymbol{B}_{\text{eq}}), \end{cases} \tag{2.6a}$$

$$\text{kinetics} \quad \begin{cases} \dfrac{\partial f_{\text{h}}}{\partial t} + \boldsymbol{v} \cdot \nabla f_{\text{h}} + (\boldsymbol{B} \times \tilde{\boldsymbol{U}} + \boldsymbol{v} \times \boldsymbol{B}) \cdot \nabla_{\boldsymbol{v}} f_{\text{h}} = 0, \\ \rho_{\text{h}} = \displaystyle\int_{\mathbb{R}^3} f_{\text{h}} \, \mathrm{d}^3 v, \qquad \boldsymbol{J}_{\text{h}} = \int_{\mathbb{R}^3} \boldsymbol{v} f_{\text{h}} \, \mathrm{d}^3 v. \end{cases} \tag{2.6b}$$

The linearization of MHD part has the consequence that the original Hamiltonian (2.2) is no longer conserved. However, the quantity

$$\mathcal{H}_1(t) = \frac{1}{2} \int_\Omega \rho_{\text{eq}} \tilde{\boldsymbol{U}}^2 \, \mathrm{d}^3 x + \frac{1}{\gamma - 1} \int_\Omega \tilde{p} \, \mathrm{d}^3 x + \frac{1}{2} \int_\Omega \tilde{\boldsymbol{B}}^2 \, \mathrm{d}^3 x + \frac{1}{2} \int_\Omega \int_{\mathbb{R}^3} \boldsymbol{v}^2 f_{\text{h}} \, \mathrm{d}^3 v \, \mathrm{d}^3 x, \tag{2.7}$$

evolves in time as

$$\begin{aligned} \frac{\mathrm{d}\mathcal{H}_1}{\mathrm{d}t} &= \int_\Omega \tilde{\boldsymbol{U}} \cdot \Big[(\nabla \times \boldsymbol{B}_{\text{eq}}) \times \tilde{\boldsymbol{B}} \Big] \, \mathrm{d}^3 x - \int_\Omega \tilde{\boldsymbol{U}} \cdot \nabla \tilde{p} \, \mathrm{d}^3 x - \int_\Omega p_{\text{eq}} \nabla \cdot \tilde{\boldsymbol{U}} \, \mathrm{d}^3 x \\ &= \int_\Omega \tilde{\boldsymbol{U}} \cdot \Big[(\nabla \times \boldsymbol{B}_{\text{eq}}) \times \tilde{\boldsymbol{B}} \Big] \, \mathrm{d}^3 x - \int_\Omega (p_{\text{eq}} - \tilde{p}) \nabla \cdot \tilde{\boldsymbol{U}} \, \mathrm{d}^3 x, \end{aligned} \tag{2.8}$$

if we assume that nothing flows in or out at the boundary $\partial\Omega$. Consequently, $\mathcal{H}_1$ is conserved for incompressible waves ($\nabla \cdot \tilde{\boldsymbol{U}} = 0$) and if additionally $\nabla \times \boldsymbol{B}_{\text{eq}} = 0$. The former is particularly true for shear Alfvén waves.

2.3 MHD equations in curvilinear coordinates

As a preparation for the application of the framework of *finite element exterior calculus* (FEEC), we reformulate (2.6a) in terms of differential forms upon which FEEC is built. For this, we first introduce a smooth, invertible coordinate transformation (to which we refer to as mapping) $\boldsymbol{F} : \hat{\Omega} \to \Omega$, $\boldsymbol{\eta} \mapsto \boldsymbol{F}(\boldsymbol{\eta}) = \boldsymbol{x}$, from a box-shaped logical domain $\hat{\Omega} = [0,1]^3$ to the physical domain $\Omega \subset \mathbb{R}^3$. Moreover, we denote by $\boldsymbol{\eta} = (\eta_1, \eta_2, \eta_3) \in \hat{\Omega}$ and $\boldsymbol{x} = (x, y, z) \in \Omega$ the logical and Cartesian coordinates, respectively. This coordinate transformation induces the Jacobian matrix

$$DF : \hat{\Omega} \to \mathbb{R}^{3\times 3}, \qquad (DF)_{ij} = \frac{\partial F_i}{\partial \eta_j}. \tag{2.9}$$

The columns of DF define local basis vectors tangent to the coordinate lines at $\boldsymbol{x} \in \Omega$ which span the tangent space denoted by $T_{\boldsymbol{x}}\Omega$. The components of a *contravariant vector* $\mathsf{a} \in T_{\boldsymbol{x}}\Omega$ (to which we refer to as *vector*) in curvilinear (or logical) coordinates, denoted by $\hat{\boldsymbol{a}}$, are defined by the relation

$\boldsymbol{a}(\boldsymbol{F}(\boldsymbol{\eta})) = DF(\boldsymbol{\eta})\hat{\boldsymbol{a}}(\boldsymbol{\eta})$, where $\boldsymbol{a}$ are the components of a vector in Cartesian coordinates[2]. Scalar fields transform as $a(\boldsymbol{F}(\boldsymbol{\eta})) = \hat{a}(\boldsymbol{\eta})$ and differential operators as

$$\nabla\phi = (DF^{-1})^\top \hat{\nabla}\hat{\phi}, \qquad \nabla\times\boldsymbol{a} = \frac{1}{\sqrt{g}} DF\,\hat{\nabla}\times(G\hat{\boldsymbol{a}}), \qquad \nabla\cdot\boldsymbol{a} = \frac{1}{\sqrt{g}}\hat{\nabla}\cdot(\sqrt{g}\hat{\boldsymbol{a}}), \tag{2.10}$$

where $\hat{\nabla} = (\partial_{\eta_1}, \partial_{\eta_2}, \partial_{\eta_3})^\top$ acts on the logical coordinates and we introduced the metric tensor along with its determinant

$$G = DF^\top DF, \qquad g = \det G = \det(DF)^2. \tag{2.11}$$

Using the identity $M\boldsymbol{b}\times M\boldsymbol{c} = \det(M)(M^{-1})^\top(\boldsymbol{b}\times\boldsymbol{c})$ with some invertible matrix $M\in\mathbb{R}^{3\times3}$, these expressions allow us to reformulate (2.6a) in curvilinear coordinates:

$$\text{MHD}\quad\begin{cases} \dfrac{\partial\hat{\rho}}{\partial t} + \dfrac{1}{\sqrt{g}}\hat{\nabla}\cdot(\sqrt{g}\hat{\rho}_{\text{eq}}\hat{\boldsymbol{U}}) = 0, & \text{(2.12a)}\\[2ex] \hat{\rho}_{\text{eq}} DF\,\dfrac{\partial\hat{\boldsymbol{U}}}{\partial t} = (DF^{-1})^\top\Big[(\hat{\nabla}\times G\hat{\boldsymbol{B}})\times\hat{\boldsymbol{B}}_{\text{eq}} + (\hat{\nabla}\times G\hat{\boldsymbol{B}}_{\text{eq}})\times\hat{\boldsymbol{B}}\Big] & \\ \qquad\qquad + (DF^{-1})^\top\Big[\sqrt{g}\,(\hat{\rho}_{\text{h}}\hat{\boldsymbol{U}} - \hat{\boldsymbol{J}}_{\text{h}})\times\hat{\boldsymbol{B}}_{\text{f}} - \hat{\nabla}\hat{p}\Big], & \text{(2.12b)}\\[2ex] \dfrac{\partial\hat{p}}{\partial t} + \dfrac{1}{\sqrt{g}}\hat{\nabla}\cdot(\sqrt{g}\,\hat{p}_{\text{eq}}\,\hat{\boldsymbol{U}}) + (\gamma-1)\hat{p}_{\text{eq}}\dfrac{1}{\sqrt{g}}\hat{\nabla}\cdot\Big(\sqrt{g}\,\hat{\boldsymbol{U}}\Big) = 0, & \text{(2.12c)}\\[2ex] DF\,\dfrac{\partial\hat{\boldsymbol{B}}}{\partial t} = \dfrac{1}{\sqrt{g}} DF\left[\hat{\nabla}\times(\hat{\boldsymbol{U}}\times\sqrt{g}\hat{\boldsymbol{B}}_{\text{eq}})\right]. & \text{(2.12d)} \end{cases}$$

Here, $\hat{\boldsymbol{B}}_{\text{f}}$ denotes the full magnetic field (equilibrium + perturbation) and we dropped the tildes for the perturbed quantities for reasons of clarity.

2.4 MHD in terms of differential forms

In order to apply the framework of FEEC, we must rewrite (2.12) in terms of differential forms. A selective collection of formulae regarding differential forms can be found in Appendix A. We refer to [16, 2] for a thorough introduction to the subject. We shall give a brief introduction in the following.

Scalar fields $\hat{a} = \hat{a}(\boldsymbol{\eta})$ and vector fields $\mathsf{a}\in T\Omega$[3] with components $\hat{\boldsymbol{a}} = \hat{\boldsymbol{a}}(\boldsymbol{\eta})$ can be related to differential p-forms $a^p \in \Lambda^p(\Omega) : T\Omega\times\cdots\times T\Omega\to\mathbb{R}$, $p\in\{0,1,2,3\}$ with components $\hat{\boldsymbol{a}}^p = \hat{\boldsymbol{a}}^p(\boldsymbol{\eta})$ in the following way:

$$a^0 = \hat{a}^0, \qquad \leftrightarrow \qquad \hat{a}^0 = \hat{a}, \tag{2.13a}$$

$$a^1 = \hat{a}^1_1\,\mathrm{d}\eta^1 + \hat{a}^1_2\,\mathrm{d}\eta^2 + \hat{a}^1_3\,\mathrm{d}\eta^3, \qquad \leftrightarrow \qquad \hat{\boldsymbol{a}}^1 = \begin{pmatrix}\hat{a}^1_1\\ \hat{a}^1_2\\ \hat{a}^1_3\end{pmatrix} = G\hat{\boldsymbol{a}}, \tag{2.13b}$$

$$a^2 = \hat{a}^2_1\,(\mathrm{d}\eta^2\wedge\mathrm{d}\eta^3) + \hat{a}^2_2\,(\mathrm{d}\eta^3\wedge\mathrm{d}\eta^1) + \hat{a}^2_3\,(\mathrm{d}\eta^1\wedge\mathrm{d}\eta^2), \qquad \leftrightarrow \qquad \hat{\boldsymbol{a}}^2 = \begin{pmatrix}\hat{a}^2_1\\ \hat{a}^2_2\\ \hat{a}^2_3\end{pmatrix} = \sqrt{g}\,\hat{\boldsymbol{a}}, \tag{2.13c}$$

$$a^3 = \hat{a}^3\,(\mathrm{d}\eta^1\wedge\mathrm{d}\eta^2\wedge\mathrm{d}\eta^3), \qquad \leftrightarrow \qquad \hat{a}^3 = \sqrt{g}\,\hat{a}. \tag{2.13d}$$

(2.13b) is the defining relation for the *sharp*-operator

$$\sharp : \Lambda^1(\Omega)\to T\Omega, \quad \hat{\boldsymbol{a}}^1 \mapsto G^{-1}\hat{\boldsymbol{a}}^1 = \hat{\boldsymbol{a}}, \tag{2.14}$$

[2]From now on, all quantities defined on the logical domain $\hat{\Omega}$ are denoted by hats, i.e. $\hat{(\cdot)}$. Moreover, we will always assume that such quantities are smooth functions of the logical coordinates $\boldsymbol{\eta}$.

[3]$T\Omega$ denotes the bundle, that is, the union of all tangent spaces $T_{\boldsymbol{x}}\Omega \quad \forall \boldsymbol{x}\in\Omega$

which transforms a differential 1-form to a vector field. In (2.13b), $\mathrm{d}\eta^\mu$ ($\mu \in \{1,2,3\}$) are the lines of the inverse Jacobian matrix DF^{-1}. They represent the *covariant* basis vectors which span the cotangent space $T^*_{\boldsymbol{x}}\Omega$ at $\boldsymbol{x} \in \Omega$, that is, the dual space of $T_{\boldsymbol{x}}\Omega$. The elements of $T^*_{\boldsymbol{x}}\Omega$ are called 1-forms. Higher-order forms are constructed via the wedge product $\wedge$ (see A.1). 0-forms are just functions on the logical domain. Let us summarize some notations regarding scalar fields, vector fields and p-forms:

- a and $\boldsymbol{a}$ denote scalar fields respectively components of vector fields in Cartesian (physical) coordinates
- $\hat{a}$ and $\hat{\boldsymbol{a}}$ denote scalar fields respectively components of vector fields in curvilinear (logical) coordinates
- a^p for $p \in \{0,1,2,3\}$ denotes a differential p-form
- $\hat{a}^p$ for $p \in \{0,3\}$ denotes the component of a 0- and 3-form, respectively
- $\hat{\boldsymbol{a}}^p$ for $p \in \{1,2\}$ denotes the components of a 1- and 2-form, respectively
- As in (2.13), we use the symbol $\leftrightarrow$ to relate a p-form to its components, e.g. $a^1 \leftrightarrow \hat{\boldsymbol{a}}^1$

A p-form can be integrated over a p-dimensional manifold. This can give some guidance of how to choose the appropriate degree of form for a physical unknown (a flux for instance, which is usually integrated over a surface, would correspond to a 2-form). But this choice is not mandatory, as a p-form can be transformed to $(3-p)$-forms by means of the Hodge-star operator $*$ (see (A.3)). Hence there are many ways of how to write (2.12) or (2.6a) in terms of differential forms. The choice can be made for purely numerical reasons, such as the implementation of boundary conditions. In this work we are guided by two main principles:

1. Keep the "frozen-in" (to the fluid velocity $\boldsymbol{U}$) equations for the mass density ρ and the magnetic field $\boldsymbol{B}$ in strong form in order to achieve strong conservation of mass and $\nabla \cdot \boldsymbol{B} = 0$ on the discrete level.
2. Write the momentum conservation law in the weak form to accommodate for the coupling to the particles via Monte-Carlo integration.

The first point leads to ρ being a 3-form and to $\boldsymbol{B}$ being a 2-form. Moreover, we choose $\boldsymbol{U}$ as a 1-form and the pressure p as a 0-form.

Upon multiplying (2.12a) with $\sqrt{g}$, (2.12b) from the left-hand side with $DF^\top$ and (2.12d) again from the left-hand side with $DF^{-1}\sqrt{g}$, respectively, and applying the relations between scalar fields and components of vector fields to components of differential forms (2.13), we obtain the following system for the components of the respective forms:

$$
\left\{
\begin{aligned}
&\frac{\partial \hat{\rho}^3}{\partial t} + \hat{\nabla} \cdot (\hat{\rho}^3_{\mathrm{eq}} G^{-1} \hat{\boldsymbol{U}}^1) = 0, && \text{(2.15a)}\\
&\frac{\hat{\rho}^3_{\mathrm{eq}}}{\sqrt{g}} \frac{\partial \hat{\boldsymbol{U}}^1}{\partial t} = \left[\hat{\nabla} \times \left(\frac{1}{\sqrt{g}} G \hat{\boldsymbol{B}}^2\right)\right] \times \left(\frac{1}{\sqrt{g}} \hat{\boldsymbol{B}}^2_{\mathrm{eq}}\right) + \left[\hat{\nabla} \times \left(\frac{1}{\sqrt{g}} G \hat{\boldsymbol{B}}^2_{\mathrm{eq}}\right)\right] \times \left(\frac{1}{\sqrt{g}} \hat{\boldsymbol{B}}^2\right) && \\
&\qquad\qquad - \frac{\hat{\rho}^3_{\mathrm{h}}}{\sqrt{g}} \left(\hat{\boldsymbol{B}}^2_{\mathrm{f}} \times G^{-1} \hat{\boldsymbol{U}}^1\right) + \frac{1}{\sqrt{g}} \left(\hat{\boldsymbol{B}}^2_{\mathrm{f}} \times \hat{\boldsymbol{J}}^2_{\mathrm{h}}\right) - \hat{\nabla} \hat{p}^0, && \text{(2.15b)}\\
&\frac{\partial \hat{p}^0}{\partial t} + \frac{1}{\sqrt{g}} \hat{\nabla} \cdot \left(\sqrt{g}\, \hat{p}^0_{\mathrm{eq}} G^{-1} \hat{\boldsymbol{U}}^1\right) + (\gamma - 1) \hat{p}^0_{\mathrm{eq}} \frac{1}{\sqrt{g}} \hat{\nabla} \cdot \left(\sqrt{g}\, G^{-1} \hat{\boldsymbol{U}}^1\right) = 0, && \text{(2.15c)}\\
&\frac{\partial \hat{\boldsymbol{B}}^2}{\partial t} = \hat{\nabla} \times \left(G^{-1} \hat{\boldsymbol{U}}^1 \times \hat{\boldsymbol{B}}^2_{\mathrm{eq}}\right). && \text{(2.15d)}
\end{aligned}
\right.
$$

The MHD equations (2.15) in terms of components of differential forms are the basis of the discretization presented in this work. Note in particular the absence the Jacobian $\sqrt{g}$ in front of the divergence and curl operators in (2.15a) and (2.15d), respectively, a fact which allows us to translate mass conservation and $\nabla \cdot \boldsymbol{B} = 0$ to the discrete level exactly (they become topological properties, independent of grid spacing and metric). Using $\mathrm{d}^3x = \sqrt{g}\,\mathrm{d}^3\eta$ which is essentially the transformation (2.13d), the MHD part of the energy (2.7) in terms of components of forms is given by

$$\mathcal{H}_{1,\mathrm{MHD}}(t) = \frac{1}{2}\int_{\hat{\Omega}} (\hat{\boldsymbol{U}}^1)^\top G^{-1} \hat{\boldsymbol{U}}^1 \sqrt{g}\,\mathrm{d}^3\eta + \frac{1}{2}\int_{\hat{\Omega}} (\hat{\boldsymbol{B}}^2)^\top G \hat{\boldsymbol{B}}^2 \frac{1}{\sqrt{g}}\,\mathrm{d}^3\eta + \frac{1}{\gamma-1}\int_{\hat{\Omega}} \hat{p}^0 \sqrt{g}\,\mathrm{d}^3\eta. \tag{2.16}$$

Finally, we can write (2.15) in a coordinate-free representation with additional operators known from differential geometry, such as the interior product (A.2) and the exterior derivative d (Table 2):

$$\frac{\partial \rho^3}{\partial t} + \mathrm{d}(i_{\sharp U^1} \rho^3_{\mathrm{eq}}) = 0, \tag{2.17a}$$

$$(*\rho^3_{\mathrm{eq}}) \wedge \frac{\partial U^1}{\partial t} = i_{\sharp * B^2_{\mathrm{eq}}} \mathrm{d} * B^2 + i_{\sharp * B^2} \mathrm{d} * B^2_{\mathrm{eq}} - (*\rho^3_{\mathrm{h}}) \wedge (i_{\sharp U^1} B^2_{\mathrm{f}}) + i_{\sharp * J^2_{\mathrm{h}}} B^2_{\mathrm{f}} - \mathrm{d}p^0, \tag{2.17b}$$

$$\frac{\partial p^0}{\partial t} - \mathrm{d}^*(p^0_{\mathrm{eq}} \wedge U^1) - (\gamma - 1) p^0_{\mathrm{eq}} \wedge \mathrm{d}^* U^1 = 0, \tag{2.17c}$$

$$\frac{\partial B^2}{\partial t} + \mathrm{d}(i_{\sharp U^1} B^2_{\mathrm{eq}}) = 0, \tag{2.17d}$$

The *co-differential* operator d^* is defined in (A.10). As shown in Table 2, the exterior derivative d acts on a 0-form as the usual grad operator on a scalar field in Cartesian coordinates. In the same way, d acts on the components of a 1-form and 2-form as the curl and div operators on components of a vector field in Cartesian coordinates, respectively.

3 Semi-discretization in space

3.1 Commuting diagram and finite element spaces

We perform the spatial dicretization of (2.15) using the framework of Finite Element Exterior Calculus (FEEC) to derive a semi-discrete system of ordinary differential equations with continuous time variable. At the heart of FEEC is the commuting diagram for function spaces depicted in Figure 1. Note that all spaces in the diagram are spaces of the components of differential forms **which are independent of the basis forms**. The infinite-dimensional spaces in the upper line are defined as

$$H^1(\hat{\Omega}) := \{\hat{a}^0 : \hat{\Omega} \to \mathbb{R}, \quad \hat{a}^0 \leftrightarrow a^0 \quad \text{s.t.} \quad (a^0, a^0) + (\mathrm{d}a^0, \mathrm{d}a^0) < \infty\}, \tag{3.1a}$$

$$H(\mathrm{curl}, \hat{\Omega}) := \{\hat{\boldsymbol{a}}^1 : \hat{\Omega} \to \mathbb{R}^3, \quad \hat{\boldsymbol{a}}^1 \leftrightarrow a^1 \quad \text{s.t.} \quad (a^1, a^1) + (\mathrm{d}a^1, \mathrm{d}a^1) < \infty\}, \tag{3.1b}$$

$$H(\mathrm{div}, \hat{\Omega}) := \{\hat{\boldsymbol{a}}^2 : \hat{\Omega} \to \mathbb{R}^3, \quad \hat{\boldsymbol{a}}^2 \leftrightarrow a^2 \quad \text{s.t.} \quad (a^2, a^2) + (\mathrm{d}a^2, \mathrm{d}a^2) < \infty\}, \tag{3.1c}$$

$$L^2(\hat{\Omega}) := \{\hat{a}^3 : \hat{\Omega} \to \mathbb{R}, \quad \hat{a}^3 \leftrightarrow a^3 \quad \text{s.t.} \quad (a^3, a^3) < \infty\}, \tag{3.1d}$$

where the action of the exterior derivative d is summarized in Table 2 and the scalar product (a^p, a^p) of p-forms is defined in (A.6). We note two important properties of the diagram:

1. Exact sequence both on the continuous and the discrete level:

$$\hat{\nabla} V_0 = \mathrm{Ker}(\hat{\nabla} \times V_1), \qquad \hat{\nabla} \times V_1 = \mathrm{Ker}(\hat{\nabla} \cdot V_2), \tag{3.2}$$

2. Commutativity:

$$\boldsymbol{\Pi}_1\,(\hat{\nabla} \hat{a}^0) = \hat{\nabla}\,(\Pi_0 \hat{a}^0), \qquad \boldsymbol{\Pi}_2\,(\hat{\nabla} \times \hat{\boldsymbol{a}}^1) = \hat{\nabla} \times\,(\boldsymbol{\Pi}_1 \hat{\boldsymbol{a}}^1), \qquad \Pi_3\,(\hat{\nabla} \cdot \hat{\boldsymbol{a}}^2) = \hat{\nabla} \cdot\,(\boldsymbol{\Pi}_2 \hat{\boldsymbol{a}}^2). \tag{3.3}$$

The first property is a consequence of the operator identities curl(grad) = 0 and div(curl) = 0.

There are multiple ways how to construct the sequence of finite element spaces $V_0, \cdots, V_3$ forming an exact de Rham sequence. In this work, we shall do this by means of tensor-products of one-dimensional B-spline basis functions introduced in [7]. We recall the construction of the spaces along

$$
\begin{tikzcd}
H^1(\hat{\Omega}) \arrow[r, "\hat{\nabla}"] \arrow[d, "\Pi_0"'] & H(\mathrm{curl}, \hat{\Omega}) \arrow[r, "\hat{\nabla}\times"] \arrow[d, "\boldsymbol{\Pi}_1"'] & H(\mathrm{div}, \hat{\Omega}) \arrow[r, "\hat{\nabla}\cdot"] \arrow[d, "\boldsymbol{\Pi}_2"'] & L^2(\hat{\Omega}) \arrow[d, "\Pi_3"'] \\
V_0 \arrow[r, "\hat{\nabla}"] & V_1 \arrow[r, "\hat{\nabla}\times"] & V_2 \arrow[r, "\hat{\nabla}\cdot"] & V_3
\end{tikzcd}
$$

Figure 1: Commuting diagram for function spaces in three space dimensions. The upper line represents the continuous, infinite-dimensional function spaces for components of p-forms (3.1) and the lower line finite-dimensional sub-spaces $V_0, \cdots, V_3$. Due to the properties curl(grad) = 0 and div(curl) = 0, both lines form an exact de Rham sequence. The link between the two sequences is made by the projection operators $\Pi_0 : H^1(\hat{\Omega}) \to V_0$, $\boldsymbol{\Pi}_1 : H(\mathrm{curl}, \hat{\Omega}) \to V_1$, $\boldsymbol{\Pi}_2 : H(\mathrm{div}, \hat{\Omega}) \to V_2$ and $\Pi_3 : L^2(\hat{\Omega}) \to V_3$ onto the finite element spaces, which must be chosen such that the diagram becomes commuting.

with commuting projection operators in Section 3.4. We denote the total number of basis functions in each space by N^n with $n \in \{0, 1, 2, 3\}$ and the number of basis functions for each component of the two vector-valued spaces by N^n_μ for $n \in \{1, 2\}$ and $\mu = \{1, 2, 3\}$ such that $N^n = N^n_1 + N^n_2 + N^n_3$ for $n \in \{1, 2\}$. This yields the following finite element spaces and approximate components of forms denoted by the subscript h:

$$
V_0 := \mathrm{span}\left\{\Lambda^0_i \,|\, 0 \le i < N^0\right\}, \qquad \hat{p}^0_h(t, \boldsymbol{\eta}) = \sum_{i=0}^{N^0-1} p_i(t)\Lambda^0_i(\boldsymbol{\eta}), \tag{3.4a}
$$

$$
V_1 := \mathrm{span}\left\{\begin{pmatrix}\Lambda^1_{1,i}\\0\\0\end{pmatrix}, \begin{pmatrix}0\\\Lambda^1_{2,i}\\0\end{pmatrix}, \begin{pmatrix}0\\0\\\Lambda^1_{3,i}\end{pmatrix} \middle| \begin{matrix}0 \le i < N^1_1\\0 \le i < N^1_2\\0 \le i < N^1_3\end{matrix}\right\}, \qquad \hat{\boldsymbol{U}}^1_h(t, \boldsymbol{\eta}) = \sum_{\mu=1}^{3}\sum_{i=0}^{N^1_\mu-1} u_{\mu,i}(t)\Lambda^1_{\mu,i}(\boldsymbol{\eta})\boldsymbol{e}_\mu \tag{3.4b}
$$

$$
V_2 := \mathrm{span}\left\{\begin{pmatrix}\Lambda^2_{1,i}\\0\\0\end{pmatrix}, \begin{pmatrix}0\\\Lambda^2_{2,i}\\0\end{pmatrix}, \begin{pmatrix}0\\0\\\Lambda^2_{3,i}\end{pmatrix} \middle| \begin{matrix}0 \le i < N^2_1\\0 \le i < N^2_2\\0 \le i < N^2_3\end{matrix}\right\}, \qquad \hat{\boldsymbol{B}}^2_h(t, \boldsymbol{\eta}) = \sum_{\mu=1}^{3}\sum_{i=0}^{N^2_\mu-1} b_{\mu,i}(t)\Lambda^2_{\mu,i}(\boldsymbol{\eta})\boldsymbol{e}_\mu \tag{3.4c}
$$

$$
V_3 := \mathrm{span}\left\{\Lambda^3_i \,|\, 0 \le i < N^3\right\}, \qquad \hat{\rho}^3_h(t, \boldsymbol{\eta}) = \sum_{i=0}^{N^3-1} \rho_i(t)\Lambda^3_i(\boldsymbol{\eta}), \tag{3.4d}
$$

Here, $\boldsymbol{e}_1 = (1, 0, 0)^\top$, $\boldsymbol{e}_2 = (0, 1, 0)^\top$ and $\boldsymbol{e}_3 = (0, 0, 1)^\top$. To simplify the notation, we stack the finite element coefficients and basis functions in column vectors, e.g. $\mathbf{p} := (\hat{p}_i)_{0 \le i < N^0} \in \mathbb{R}^{N^0}$ and $\boldsymbol{\Lambda}^0 := (\Lambda^0_i)_{0 \le i < N^0} \in \mathbb{R}^{N^0}$. The right-hand sides of (3.4) can then compactly written as

$$
\hat{p}^0_h = (p, \cdots, p_{N^0-1})\begin{pmatrix}\Lambda^0_0\\\vdots\\\Lambda^0_{N^0-1}\end{pmatrix} =: \mathbf{p}^\top\boldsymbol{\Lambda}^0, \tag{3.5a}
$$

$$
(\hat{\boldsymbol{U}}^1_h)^\top = (\underbrace{u_{1,0}, \cdots, u_{1,N^1_1-1}}_{=:\mathbf{u}_1^\top}, \underbrace{u_{2,0}, \cdots, u_{2,N^1_2-1}}_{=:\mathbf{u}_2^\top}, \underbrace{u_{3,0}, \cdots, u_{3,N^1_3-1}}_{=:\mathbf{u}_3^\top})\begin{pmatrix}\boldsymbol{\Lambda}^1_1 & 0 & 0\\0 & \boldsymbol{\Lambda}^1_2 & 0\\0 & 0 & \boldsymbol{\Lambda}^1_3\end{pmatrix} =: \mathbf{u}^\top\mathbb{\Lambda}^1, \tag{3.5b}
$$

$$
(\hat{\boldsymbol{B}}^2_h)^\top = (\underbrace{b_{1,0}, \cdots, b_{1,N^2_1-1}}_{=:\mathbf{b}_1^\top}, \underbrace{b_{2,0}, \cdots, b_{2,N^2_2-1}}_{=:\mathbf{b}_2^\top}, \underbrace{b_{3,0}, \cdots, b_{3,N^2_3-1}}_{=:\mathbf{b}_3^\top})\begin{pmatrix}\boldsymbol{\Lambda}^2_1 & 0 & 0\\0 & \boldsymbol{\Lambda}^2_2 & 0\\0 & 0 & \boldsymbol{\Lambda}^2_3\end{pmatrix} =: \mathbf{b}^\top\mathbb{\Lambda}^2, \tag{3.5c}
$$

$$
\hat{\rho}^3_h = (\rho_0, \ldots, \rho_{N^3-1})\begin{pmatrix}\Lambda^3_0\\\vdots\\\Lambda^3_{N^3-1}\end{pmatrix} =: \boldsymbol{\rho}^\top\boldsymbol{\Lambda}^3, \tag{3.5d}
$$

such that $\mathbb{\Lambda}^1 \in \mathbb{R}^{N^1\times 3}$ and $\mathbb{\Lambda}^2 \in \mathbb{R}^{N^2\times 3}$. Moreover, we introduce discrete representations of the exterior derivative which are matrices solely acting on finite element coefficients, e.g.

$$\hat{\nabla}\hat{p}^0_h = (\mathbb{G}\mathbf{p})^\top \mathbb{\Lambda}^1, \qquad \hat{\nabla}\times\hat{\boldsymbol{U}}^1_h = (\mathbb{C}\mathbf{u})^\top\mathbb{\Lambda}^2, \qquad \hat{\nabla}\cdot\hat{\boldsymbol{B}}^2_h = (\mathbb{D}\mathbf{b})^\top\boldsymbol{\Lambda}^3, \tag{3.6}$$

where $\mathbb{G}\in\mathbb{R}^{N^1\times N^0}$, $\mathbb{C}\in\mathbb{R}^{N^2\times N^1}$ and $\mathbb{D}\in\mathbb{R}^{N^3\times N^2}$ satisfying $\mathbb{C}\mathbb{G}=0$ and $\mathbb{D}\mathbb{C}=0$. Their explicit form using tensor-product B-spline basis functions will be shown Section 3.4. Finally, we introduce the following symmetric mass matrices in each of the four discrete spaces which follow from the definitions of the L^2-inner products (A.6):

$$\mathbb{M}^0 := \int_{\hat{\Omega}} \boldsymbol{\Lambda}^0(\boldsymbol{\Lambda}^0)^\top\sqrt{g}\,\mathrm{d}^3\eta, \qquad \in\mathbb{R}^{N^0\times N^0}. \tag{3.7a}$$

$$\mathbb{M}^1 := \int_{\hat{\Omega}} \mathbb{\Lambda}^1 G^{-1}(\mathbb{\Lambda}^1)^\top\sqrt{g}\,\mathrm{d}^3\eta, \qquad \in\mathbb{R}^{N^1\times N^1}, \tag{3.7b}$$

$$\mathbb{M}^2 := \int_{\hat{\Omega}} \mathbb{\Lambda}^2 G(\mathbb{\Lambda}^2)^\top\frac{1}{\sqrt{g}}\,\mathrm{d}^3\eta, \qquad \in\mathbb{R}^{N^2\times N^2}, \tag{3.7c}$$

$$\mathbb{M}^3 := \int_{\hat{\Omega}} \boldsymbol{\Lambda}^3(\boldsymbol{\Lambda}^3)^\top\frac{1}{\sqrt{g}}\,\mathrm{d}^3\eta, \qquad \in\mathbb{R}^{N^3\times N^3}. \tag{3.7d}$$

3.2 Strong equations: mass continuity and induction equation

As already indicated in Section 2.4, we keep the mass conservation law and induction equation in strong form to achieve point-wise conservation of mass and $\nabla\cdot\boldsymbol{B}=0$. Hence we take (2.15a), project it on the space V_3, make use of the commutativity relations (3.3), replace $\hat{\boldsymbol{U}}^1$ by its approximation $\hat{\boldsymbol{U}}^1_h$ and insert the expansions (3.5b) and (3.5d) in the respective basis:

$$\frac{\partial\hat{\rho}^3_h}{\partial t} + \hat{\nabla}\cdot\boldsymbol{\Pi}_2\left[\hat{\rho}^3_{\mathrm{eq}}G^{-1}\hat{\boldsymbol{U}}^1_h\right] = 0, \tag{3.8}$$

$$\Leftrightarrow \quad (\boldsymbol{\Lambda}^3)^\top\frac{\mathrm{d}\boldsymbol{\rho}}{\mathrm{d}t} + (\boldsymbol{\Lambda}^3)^\top\mathbb{D}\,\tilde{\boldsymbol{\Pi}}_2\left[\hat{\rho}^3_{\mathrm{eq}}G^{-1}(\mathbb{\Lambda}^1)^\top\right]\mathbf{u} = 0, \tag{3.9}$$

$$\Leftrightarrow \quad \frac{\mathrm{d}\boldsymbol{\rho}}{\mathrm{d}t} + \mathbb{D}\mathcal{Q}\mathbf{u} = 0. \tag{3.10}$$

Moreover, in the last line, we introduced the projection matrix $\mathcal{Q}\in\mathbb{R}^{N^2\times N^1}$ which can be seen as a matrix containing all coefficients in the space V_2 (lines) of all projected basis functions in V_1 weighted with some quantity (columns), here the equilibrium 3-form density multiplied by the inverse metric tensor G^{-1}. Explicitly,

$$\mathcal{Q} := \left(\tilde{\boldsymbol{\Pi}}_2\left[\hat{\rho}^3_{\mathrm{eq}}G^{-1}\begin{pmatrix}\Lambda^1_{1,i}\\0\\0\end{pmatrix}\right]_{0\le i<N^1_1}, \tilde{\boldsymbol{\Pi}}_2\left[\hat{\rho}^3_{\mathrm{eq}}G^{-1}\begin{pmatrix}0\\\Lambda^1_{2,i}\\0\end{pmatrix}\right]_{0\le i<N^1_2}, \tilde{\boldsymbol{\Pi}}_2\left[\hat{\rho}^3_{\mathrm{eq}}G^{-1}\begin{pmatrix}0\\0\\\Lambda^1_{3,i}\end{pmatrix}\right]_{0\le i<N^1_3}\right). \tag{3.11}$$

We place a tilde over the projectors, e.g. $\tilde{\Pi}_3$, to indicate the restriction to the coefficients of a projection, excluding the basis functions, e.g. $\Pi_3\hat{\rho}^3 = \hat{\rho}^3_h = (\boldsymbol{\Lambda}^3)^\top\boldsymbol{\rho}\in V_3$ but $\tilde{\Pi}_3\hat{\rho}^3 = \boldsymbol{\rho}\in\mathbb{R}^{N^3}$. Regarding conservation of the discrete mass M_h, we note that

$$\frac{\mathrm{d}M_h}{\mathrm{d}t} = \int_{\hat{\Omega}}\hat{\rho}^3_h\,\mathrm{d}^3\eta = \left(\frac{\mathrm{d}\boldsymbol{\rho}}{\mathrm{d}t}\right)^\top\int_{\hat{\Omega}}\boldsymbol{\Lambda}^3\,\mathrm{d}^3\eta = -\mathbf{u}^\top\mathcal{Q}^\top\mathbb{D}^\top\int_{\hat{\Omega}}\boldsymbol{\Lambda}^3\,\mathrm{d}^3\eta = 0, \tag{3.12}$$

since the basis functions in V_3 are all normalized to one in case of the B-spline construction shown in Section 3.4 and the corresponding discrete divergence matrix $\mathbb{D}$ takes the difference of two neighboring values of the vector it is applied to.

In the same way, we obtain for the induction equation (2.15d)

$$
\begin{aligned}
&& \frac{\partial \hat{\boldsymbol{B}}_h^2}{\partial t} + \hat{\nabla} \times \boldsymbol{\Pi}_1 \left[\mathbb{B}_{\text{eq}} G^{-1} \hat{\boldsymbol{U}}_h^1\right] = 0, && (3.13)\\
\Leftrightarrow && (\boldsymbol{\Lambda}^2)^\top \frac{\mathrm{d}\mathbf{b}}{\mathrm{d}t} + (\boldsymbol{\Lambda}^2)^\top \mathbb{C}\, \tilde{\boldsymbol{\Pi}}_1 \left[\mathbb{B}_{\text{eq}} G^{-1} (\mathbb{\Lambda}^1)^\top\right] \mathbf{u} = 0, && (3.14)\\
\Leftrightarrow && \frac{\mathrm{d}\mathbf{b}}{\mathrm{d}t} + \mathbb{C}\mathcal{T}\mathbf{u} = 0, && (3.15)
\end{aligned}
$$

where we wrote the cross product of the background magnetic field with another vector in terms of a matrix-vector product by using the anti-symmetric matrix

$$
\mathbb{B}_{\text{eq}} := \begin{pmatrix} 0 & -\hat{B}_{\text{eq},3} & \hat{B}_{\text{eq},2} \\ \hat{B}_{\text{eq},3} & 0 & -\hat{B}_{\text{eq},1} \\ -\hat{B}_{\text{eq},2} & \hat{B}_{\text{eq},1} & 0 \end{pmatrix} \in \mathbb{R}^{3\times 3}. \tag{3.16}
$$

Moreover, we introduced another projection matrix $\mathcal{T} \in \mathbb{R}^{N^1 \times N^1}$:

$$
\mathcal{T} := \left(\tilde{\boldsymbol{\Pi}}_1 \left[\mathbb{B}_{\text{eq}} G^{-1} \begin{pmatrix} \Lambda^1_{1,i} \\ 0 \\ 0 \end{pmatrix}\right]_{0\le i<N_1^1}, \tilde{\boldsymbol{\Pi}}_1 \left[\mathbb{B}_{\text{eq}} G^{-1} \begin{pmatrix} 0 \\ \Lambda^1_{2,i} \\ 0 \end{pmatrix}\right]_{0\le i<N_2^1}, \tilde{\boldsymbol{\Pi}}_1 \left[\mathbb{B}_{\text{eq}} G^{-1} \begin{pmatrix} 0 \\ 0 \\ \Lambda^1_{3,i} \end{pmatrix}\right]_{0\le i<N_3^1} \right). \tag{3.17}
$$

Finally, we note that (3.15) preserves the zero-divergence constraint for the magnetic field,

$$
\frac{\partial}{\partial t}(\hat{\nabla} \cdot \hat{\boldsymbol{B}}_h^2) = \left(\mathbb{D}\frac{\mathrm{d}\mathbf{b}}{\mathrm{d}t}\right)^\top \boldsymbol{\Lambda}^3 = -(\mathbb{D}\mathbb{C}\mathcal{T}\mathbf{u})^\top \boldsymbol{\Lambda}^3 = 0, \tag{3.18}
$$

due to $\mathbb{D}\mathbb{C} = 0$, a consequence of the special choice of compatible finite element spaces forming an exact de Rham sequence. The satisfaction of the zero-divergence constraint at $t = 0$ is ensured by the commuting diagram property:

$$
\hat{\nabla} \cdot \hat{\boldsymbol{B}}_h^2(t=0) = \hat{\nabla} \cdot \boldsymbol{\Pi}_2 \hat{\boldsymbol{B}}^2(t=0) = \Pi_3 \left[\hat{\nabla} \cdot \hat{\boldsymbol{B}}^2(t=0)\right] = 0. \tag{3.19}
$$

An example is shown in Section 3.4.

3.3 Weak equations: momentum conservation and pressure

We choose a weak formulation for the momentum balance equation (2.15b). Consequently, we take the L^2-inner product of 1-forms defined in (A.6) with a test function $\hat{\boldsymbol{C}}^1 \in H(\text{curl}, \hat{\Omega})$:

$$
\begin{aligned}
\int_{\hat{\Omega}} \frac{\hat{\rho}^3_{\text{eq}}}{\sqrt{g}} \left(\frac{\partial \hat{\boldsymbol{U}}^1}{\partial t}\right)^\top G^{-1} \hat{\boldsymbol{C}}^1 \sqrt{g}\, \mathrm{d}^3\eta &= \int_{\hat{\Omega}} \left\{ \left[\hat{\nabla} \times \left(\frac{1}{\sqrt{g}} G \hat{\boldsymbol{B}}^2\right)\right] \times \left(\frac{1}{\sqrt{g}} \hat{\boldsymbol{B}}^2_{\text{eq}}\right)\right\}^\top G^{-1} \hat{\boldsymbol{C}}^1 \sqrt{g}\, \mathrm{d}^3\eta \\
&+ \int_{\hat{\Omega}} \left\{ \left[\hat{\nabla} \times \left(\frac{1}{\sqrt{g}} G \hat{\boldsymbol{B}}^2_{\text{eq}}\right)\right] \times \left(\frac{1}{\sqrt{g}} \hat{\boldsymbol{B}}^2\right)\right\}^\top G^{-1} \hat{\boldsymbol{C}}^1 \sqrt{g}\, \mathrm{d}^3\eta \\
&- \int_{\hat{\Omega}} (\hat{\nabla}\hat{p}^0)^\top G^{-1} \hat{\boldsymbol{C}}^1 \sqrt{g}\, \mathrm{d}^3\eta \\
&- \underbrace{\int_{\hat{\Omega}} \frac{\hat{\rho}^3_{\text{h}}}{\sqrt{g}} \left(\hat{\boldsymbol{B}}^2_{\text{f}} \times G^{-1} \hat{\boldsymbol{U}}^1\right)^\top G^{-1} \hat{\boldsymbol{C}}^1 \sqrt{g}\, \mathrm{d}^3\eta}_{:= \text{CC}(\rho_{\text{ch}})} \\
&+ \underbrace{\int_{\hat{\Omega}} \frac{1}{\sqrt{g}} \left(\hat{\boldsymbol{B}}^2_{\text{f}} \times \hat{\boldsymbol{J}}^2_{\text{h}}\right)^\top G^{-1} \hat{\boldsymbol{C}}^1 \sqrt{g}\, \mathrm{d}^3\eta}_{:= \text{CC}(\boldsymbol{J}_{\text{h}})} \qquad \forall \hat{\boldsymbol{C}}^1 \in H(\text{curl}, \hat{\Omega}).
\end{aligned} \tag{3.20}
$$

The last two terms $\mathrm{CC}(\rho_\mathrm{h})$ and $\mathrm{CC}(\boldsymbol{J}_\mathrm{h})$ involving the coupling to the kinetic species via the charge density ρ_h and the current density $\boldsymbol{J}_\mathrm{h}$ are treated separately in Section 3.5. From an energy conservation point of view, the inertia term on the left-hand side and the first Lorentz-force term on the right-hand side are in particular important. Regarding the latter, we use $\boldsymbol{a}\cdot(\boldsymbol{b}\times\boldsymbol{c}) = \boldsymbol{c}\cdot(\boldsymbol{a}\times\boldsymbol{b})$ and integrate by parts (assuming the boundary term vanishes) to obtain

$$\begin{aligned}\int_{\hat\Omega}\left\{\left[\hat\nabla\times\left(\frac{1}{\sqrt{g}}G\hat{\boldsymbol{B}}^2\right)\right]\times\left(\frac{1}{\sqrt{g}}\hat{\boldsymbol{B}}^2_\mathrm{eq}\right)\right\}^\top G^{-1}\hat{\boldsymbol{C}}^1\sqrt{g}\,\mathrm{d}^3\eta = \\ \int_{\hat\Omega}\left(\frac{1}{\sqrt{g}}G\hat{\boldsymbol{B}}^2\right)^\top\hat\nabla\times\left(\hat{\boldsymbol{B}}^2_\mathrm{eq}\times G^{-1}\hat{\boldsymbol{C}}^1\right)\mathrm{d}^3\eta.\end{aligned} \tag{3.21}$$

We recognize the symmetry to the induction equation (2.15d) if we set $\hat{\boldsymbol{C}}^1 = \hat{\boldsymbol{U}}^1$ and if the induction equation is tested with $\hat{\boldsymbol{B}}^2$ via the scalar product of 2-forms.

In order to obtain a discrete version of (3.20), we make use of the projectors $\boldsymbol{\Pi}_1$ and $\boldsymbol{\Pi}_2$ and approximate scalar products of 1-forms and 2-forms, respectively, by

$$(a^1,b^1) = \int_{\hat\Omega}(\hat{\boldsymbol{a}}^1)^\top G^{-1}\hat{\boldsymbol{b}}^1\sqrt{g}\,\mathrm{d}^3\eta \approx \int_{\hat\Omega}(\boldsymbol{\Pi}_1\hat{\boldsymbol{a}}^1)^\top G^{-1}(\boldsymbol{\Pi}_1\hat{\boldsymbol{b}}^1)\sqrt{g}\,\mathrm{d}^3\eta, \tag{3.22}$$

$$(a^2,b^2) = \int_{\hat\Omega}(\hat{\boldsymbol{a}}^2)^\top G\hat{\boldsymbol{b}}^2\frac{1}{\sqrt{g}}\,\mathrm{d}^3\eta \approx \int_{\hat\Omega}(\boldsymbol{\Pi}_2\hat{\boldsymbol{a}}^2)^\top G(\boldsymbol{\Pi}_2\hat{\boldsymbol{b}}^2)\frac{1}{\sqrt{g}}\,\mathrm{d}^3\eta. \tag{3.23}$$

For reasons of conservation of energy, we take the following average for the inertia term on the left-hand side of (3.20):

$$\begin{aligned}\int_{\hat\Omega}\frac{\hat\rho^3_\mathrm{eq}}{\sqrt{g}}\left(\frac{\partial\hat{\boldsymbol{U}}^1}{\partial t}\right)^\top G^{-1}\hat{\boldsymbol{C}}^1\sqrt{g}\,\mathrm{d}^3\eta \approx \frac{1}{2}\int_{\hat\Omega}\left[\boldsymbol{\Pi}_1\left(\frac{\hat\rho^3_\mathrm{eq}}{\sqrt{g}}\frac{\partial\hat{\boldsymbol{U}}^1_h}{\partial t}\right)\right]^\top G^{-1}\hat{\boldsymbol{C}}^1_h\sqrt{g}\,\mathrm{d}^3\eta \\ +\frac{1}{2}\int_{\hat\Omega}\left(\frac{\partial\hat{\boldsymbol{U}}^1}{\partial t}\right)^\top G^{-1}\boldsymbol{\Pi}_1\left(\frac{\hat\rho^3_\mathrm{eq}}{\sqrt{g}}\hat{\boldsymbol{C}}^1_h\right)\sqrt{g}\,\mathrm{d}^3\eta.\end{aligned} \tag{3.24}$$

Expanding $\hat{\boldsymbol{U}}^1_h$ and $\hat{\boldsymbol{C}}^1_h$ in the basis of V_1 yields

$$\int_{\hat\Omega}\left(\frac{\partial\hat{\boldsymbol{U}}^1}{\partial t}\right)^\top G^{-1}\boldsymbol{\Pi}_1\left(\frac{\hat\rho^3_\mathrm{eq}}{\sqrt{g}}\hat{\boldsymbol{C}}^1_h\right)\sqrt{g}\,\mathrm{d}^3\eta = \left(\frac{\mathrm{d}\mathbf{u}}{\mathrm{d}t}\right)^\top\underbrace{\int_{\hat\Omega}\mathbb{\Lambda}^1 G^{-1}(\mathbb{\Lambda}^1)^\top\sqrt{g}\,\mathrm{d}^3\eta}_{=\mathbb{M}^1}\,\tilde{\boldsymbol{\Pi}}_1\left[\frac{\hat\rho^3_\mathrm{eq}}{\sqrt{g}}(\mathbb{\Lambda}^1)^\top\right]\mathbf{c}. \tag{3.25}$$

We recognize the mass matrix $\mathbb{M}^1$ and another projection matrix $\mathcal{W}\in\mathbb{R}^{N^1\times N^1}$ defined as

$$\mathcal{W} := \left(\tilde{\boldsymbol{\Pi}}_1\left[\frac{\hat\rho^3_\mathrm{eq}}{\sqrt{g}}\begin{pmatrix}\Lambda^1_{1,i}\\0\\0\end{pmatrix}\right]_{0\le i<N^1_1},\tilde{\boldsymbol{\Pi}}_1\left[\frac{\hat\rho^3_\mathrm{eq}}{\sqrt{g}}\begin{pmatrix}0\\\Lambda^1_{2,i}\\0\end{pmatrix}\right]_{0\le i<N^1_2},\tilde{\boldsymbol{\Pi}}_1\left[\frac{\hat\rho^3_\mathrm{eq}}{\sqrt{g}}\begin{pmatrix}0\\0\\\Lambda^1_{3,i}\end{pmatrix}\right]_{0\le i<N^1_3}\right). \tag{3.26}$$

Note that $\mathcal{W}$ is the identity times a constant value if $\rho_\mathrm{eq} = \hat\rho^3_\mathrm{eq}/\sqrt{g}$ is independent of $\boldsymbol{\eta}$. Finally, the inertia term is discretized as

$$\int_{\hat\Omega}\frac{\hat\rho^3_\mathrm{eq}}{\sqrt{g}}\left(\frac{\partial\hat{\boldsymbol{U}}^1}{\partial t}\right)^\top G^{-1}\hat{\boldsymbol{C}}^1\sqrt{g}\,\mathrm{d}^3\eta \approx \left(\frac{\mathrm{d}\mathbf{u}}{\mathrm{d}t}\right)^\top\frac{1}{2}(\mathcal{W}^\top\mathbb{M}^1+\mathbb{M}^1\mathcal{W})\mathbf{c} =: \mathbf{c}^\top\mathcal{A}\frac{\mathrm{d}\mathbf{u}}{\mathrm{d}t}, \tag{3.27}$$

where $\mathcal{A}\in\mathbb{R}^{N^1\times N^1}$ is symmetric. Using (3.23) and the commutativity of $\boldsymbol{\Pi}_2$ and $\hat\nabla\times$, the right-hand side of (3.21) amounts to

$$\begin{aligned}\int_{\hat\Omega}(\hat{\boldsymbol{B}}^2)^\top G\hat\nabla\times\left(\hat{\boldsymbol{B}}^2_\mathrm{eq}\times G^{-1}\hat{\boldsymbol{C}}^1\right)\frac{1}{\sqrt{g}}\mathrm{d}^3\eta &\approx \int_{\hat\Omega}(\hat{\boldsymbol{B}}^2_h)^\top G\hat\nabla\times\boldsymbol{\Pi}_1\left(\hat{\boldsymbol{B}}^2_\mathrm{eq}\times G^{-1}\hat{\boldsymbol{C}}^1_h\right)\frac{1}{\sqrt{g}}\mathrm{d}^3\eta \\ &= \mathbf{b}^\top\underbrace{\int_{\hat\Omega}\mathbb{\Lambda}^2 G(\mathbb{\Lambda}^2)^\top\frac{1}{\sqrt{g}}\mathrm{d}^3\eta}_{=\mathbb{M}^2}\,\mathbb{C}\tilde{\boldsymbol{\Pi}}_1\left[\mathbb{B}_\mathrm{eq}G^{-1}(\mathbb{\Lambda}^1)^\top\right]\mathbf{c} \\ &=: \mathbf{b}^\top\mathbb{M}^2\mathbb{C}\mathcal{T}\mathbf{c},\end{aligned} \tag{3.28}$$

where $\mathcal{T}$ is the same projection matrix as in the semi-discrete induction equation (3.15). As the same techniques are applied for the remaining two terms not involving a coupling to the kinetic species, we skip the detailed derivation and just give the resulting discrete versions which read

$$\begin{aligned}\int_{\hat\Omega} \left\{\left[\hat\nabla \times \left(\frac{1}{\sqrt{g}} G \hat{\boldsymbol{B}}^2_{\text{eq}}\right)\right] \times \left(\frac{1}{\sqrt{g}}\hat{\boldsymbol{B}}^2\right)\right\}^\top & G^{-1}\hat{\boldsymbol{C}}^1\sqrt{g}\,\mathrm{d}^3\eta \\ &\approx \mathbf{b}^\top\left[\tilde{\boldsymbol{\Pi}}_1\left(\frac{1}{\sqrt{g}}\mathbb{B}^{\hat\nabla\times}_{\text{eq}}(\mathbb{\Lambda}^2)^\top\right)\right]^\top \int_{\hat\Omega}\mathbb{\Lambda}^1 G^{-1}(\mathbb{\Lambda}^1)^\top\sqrt{g}\,\mathrm{d}^3\eta\,\mathbf{c} \\ &=: \mathbf{b}^\top\mathcal{P}^\top\mathbb{M}^1\mathbf{c},\end{aligned} \tag{3.29}$$

$$\int_{\hat\Omega}(\hat\nabla\hat p^0)^\top G^{-1}\hat{\boldsymbol{C}}^1\sqrt{g}\,\mathrm{d}^3\eta \approx \mathbf{p}^\top\mathbb{G}^\top\mathbb{M}^1\mathbf{c}, \tag{3.30}$$

where $\mathcal{P}\in\mathbb{R}^{N^1\times N^2}$, given by

$$\mathcal{P} := \left(\tilde{\boldsymbol{\Pi}}_1\left[\frac{1}{\sqrt{g}}\mathbb{B}^{\hat\nabla\times}_{\text{eq}}\begin{pmatrix}\Lambda^2_{1,i}\\0\\0\end{pmatrix}\right]_{0\le i<N^2_1}, \tilde{\boldsymbol{\Pi}}_1\left[\frac{1}{\sqrt{g}}\mathbb{B}^{\hat\nabla\times}_{\text{eq}}\begin{pmatrix}0\\\Lambda^2_{2,i}\\0\end{pmatrix}\right]_{0\le i<N^2_2}, \tilde{\boldsymbol{\Pi}}_1\left[\frac{1}{\sqrt{g}}\mathbb{B}^{\hat\nabla\times}_{\text{eq}}\begin{pmatrix}0\\0\\\Lambda^2_{3,i}\end{pmatrix}\right]_{0\le i<N^2_3}\right). \tag{3.31}$$

The expression $\mathbb{B}^{\hat\nabla\times}_{\text{eq}}$ represents again the cross product in terms of a matrix vector-multiplication like (3.16) but this time built from the three components of $\hat\nabla\times(G\hat{\boldsymbol{B}}^2_{\text{eq}}/\sqrt{g})$. In summary, we end up with semi-discrete momentum balance equation

$$\mathbf{c}^\top\mathcal{A}\dot{\mathbf{u}} = \mathbf{c}^\top\mathcal{T}^\top\mathbb{C}^\top\mathbb{M}^2\mathbf{b} + \mathbf{c}^\top\mathbb{M}^1\mathcal{P}\mathbf{b} - \mathbf{c}^\top\mathbb{M}^1\mathbb{G}\mathbf{p} - \mathrm{CC}(\rho_\mathrm{h}) + \mathrm{CC}(\boldsymbol{J}_\mathrm{h}) \qquad \forall\,\mathbf{c}\in\mathbb{R}^{N^1}, \tag{3.32}$$

with $\mathrm{CC}(\rho_\mathrm{h})$ and $\mathrm{CC}(\boldsymbol{J}_\mathrm{h})$ given in Section 3.5.

We obtain the following weak formulation for the pressure equation (2.15c) by taking the 0-form scalar product from (A.6) with a test function $\hat r^0$:

$$\begin{aligned}\int_{\hat\Omega}\frac{\partial\hat p^0}{\partial t}\hat r^0\sqrt{g}\,\mathrm{d}^3\eta - \int_{\hat\Omega}\hat p^0_{\text{eq}}(\hat{\boldsymbol{U}}^1)^\top G^{-1}\hat\nabla\hat r^0\sqrt{g}\,\mathrm{d}^3\eta - (\gamma-1)\int_{\hat\Omega}(\hat{\boldsymbol{U}}^1)^\top G^{-1}\hat\nabla(\hat p^0_{\text{eq}}\hat r^0)\sqrt{g}\,\mathrm{d}^3\eta = 0 \\ \forall\,\hat r^0\in H^1(\hat\Omega).\end{aligned} \tag{3.33}$$

Here, we integrated by parts the two terms involving the divergence operator. This form is easier to handle from an implementation point of view since it requires less projections. The discrete versions of the three terms in (3.33) are given by

$$\begin{aligned}\int_{\hat\Omega}\frac{\partial\hat p^0}{\partial t}\hat r^0\sqrt{g}\,\mathrm{d}^3\eta &\approx \left(\frac{\mathrm{d}\mathbf{p}}{\mathrm{d}t}\right)^\top\int_{\hat\Omega}\boldsymbol{\Lambda}^0(\boldsymbol{\Lambda}^0)^\top\sqrt{g}\,\mathrm{d}^3\eta\,\mathbf{r} \\ &= \left(\frac{\mathrm{d}\mathbf{p}}{\mathrm{d}t}\right)^\top\mathbb{M}^0\mathbf{r},\end{aligned} \tag{3.34}$$

$$\begin{aligned}\int_{\hat\Omega}\hat p^0_{\text{eq}}(\hat{\boldsymbol{U}}^1)^\top G^{-1}\hat\nabla\hat r^0\sqrt{g}\,\mathrm{d}^3\eta &\approx \mathbf{u}^\top\left[\tilde{\boldsymbol{\Pi}}_1\left(\hat p^0_{\text{eq}}(\mathbb{\Lambda}^1)^\top\right)\right]^\top\int_{\hat\Omega}\mathbb{\Lambda}^1G^{-1}(\mathbb{\Lambda}^1)^\top\sqrt{g}\,\mathrm{d}^3\eta\,\mathbb{G}\mathbf{r} \\ &=: \mathbf{u}^\top\mathcal{S}^\top\mathbb{M}^1\mathbb{G}\mathbf{r},\end{aligned} \tag{3.35}$$

$$\begin{aligned}\int_{\hat\Omega}(\hat{\boldsymbol{U}}^1)^\top G^{-1}\hat\nabla(\hat p^0_{\text{eq}}\hat r^0)\sqrt{g}\,\mathrm{d}^3\eta &\approx \mathbf{u}^\top\int_{\hat\Omega}\mathbb{\Lambda}^1G^{-1}(\mathbb{\Lambda}^1)^\top\sqrt{g}\,\mathrm{d}^3\eta\,\mathbb{G}\tilde\Pi_0\left[\hat p^0_{\text{eq}}(\boldsymbol{\Lambda}^0)^\top\right]\mathbf{r} \\ &=: \mathbf{u}^\top\mathbb{M}^1\mathbb{G}\mathcal{K}\mathbf{r},\end{aligned} \tag{3.36}$$

with $\mathcal{S}\in\mathbb{R}^{N^1\times N^1}$ and $\mathcal{K}\in\mathbb{R}^{N^0\times N^0}$ defined as

$$\mathcal{S} := \left(\tilde{\boldsymbol{\Pi}}_1\left[\hat p^0_{\text{eq}}\begin{pmatrix}\Lambda^1_{1,i}\\0\\0\end{pmatrix}\right]_{0\le i<N^1_1}, \tilde{\boldsymbol{\Pi}}_1\left[\hat p^0_{\text{eq}}\begin{pmatrix}0\\\Lambda^1_{2,i}\\0\end{pmatrix}\right]_{0\le i<N^1_2}, \tilde{\boldsymbol{\Pi}}_1\left[\hat p^0_{\text{eq}}\begin{pmatrix}0\\0\\\Lambda^1_{3,i}\end{pmatrix}\right]_{0\le i<N^1_3}\right), \tag{3.37}$$

$$\mathcal{K} := \left(\Pi_0\left[\hat p^0_{\text{eq}}\Lambda^0_i\right]_{0\le i<N^0}\right). \tag{3.38}$$

In summary, the semi-discrete pressure equation reads

$$\mathbb{M}^0 \frac{\mathrm{d}\mathbf{p}}{\mathrm{d}t} = \mathbb{G}^\top \mathbb{M}^1 \mathcal{S}\mathbf{u} + (\gamma - 1)\mathcal{K}^\top \mathbb{G}^\top \mathbb{M}^1 \mathbf{u}, \tag{3.39}$$

due to the fact that we want each term to be true for all $\mathbf{r} \in \mathbb{R}^{N^0}$.

3.4 Example: commuting diagram with B-splines and quasi-interpolation

3.4.1 B-splines and discrete derivatives

In this section, we review the construction of the finite element spaces and projectors shown in the diagram in Figure 1 using tensor-products of univariate B-splines. B-splines are piece-wise polynomials of degree p with a compact support. A one-dimensional family of B-splines on the logical domain $\hat{\Omega} = [0,1]^3$ is fully determined by a non-decreasing sequence of points (or knots) on the real line which we collect in a vector $\hat{T} = \{\eta_i\}_{0 \leq i \leq n+2p}$ called the *knot vector*. If the knot vector contains at a point m repeated knots, ones says that this knot has multiplicity m. The i-th B-spline $\hat{N}_i^p$ of degree p is then recursively defined by

$$\hat{N}_i^p(\eta) := w_i^p(\eta)\hat{N}_i^{p-1}(\eta) + (1 - w_{i+1}^p(\eta))\hat{N}_{i+1}^{p-1}(\eta), \qquad w_i^p(\eta) := \frac{\eta - \eta_i}{\eta_{i+p} - \eta_i}, \tag{3.40a}$$

$$\hat{N}_i^0(\eta) := \begin{cases} 1, & \eta \in [\eta_i, \eta_{i+1}), \\ 0 & \text{else.} \end{cases} \tag{3.40b}$$

We note some important properties of a B-spline basis:

- B-splines are piece-wise polynomials of degree p,
- B-splines are non-negative,
- Compact support: the support of $\hat{N}_i^p$ is contained in $[\eta_i, \cdots, \eta_{i+p+1})$,
- Partition of unity: $\sum_i \hat{N}_i^p(\eta) = 1, \; \forall \, \eta \in [0,1]$,
- Local linear independence,
- If a knot η_i has multiplicity m then $\hat{N}_i^p \in C^{p-m}$ at η_i.

In this work, we shall consider two types of knot vectors yielding either a uniform, *clamped* basis or a uniform, periodic basis. The knot vectors are constructed from a uniform partition of the domain $\hat{\Omega} = [0,1]$ into n elements of equal length h and certain extensions at the boundaries to obtain the two different types:

$$\text{clamped}: \quad \hat{T} = \{\underbrace{0, \cdots, 0}_{p \text{ times}}, \underbrace{0, h, 2h, \cdots, 1-2h, 1-h, 1}_{n+1 \text{ element boundaries}}, \underbrace{1, \cdots, 1}_{p \text{ times}}\}, \tag{3.41}$$

$$\text{periodic}: \quad \hat{T} = \{\underbrace{-ph, \cdots, -h}_{p \text{ terms}}, \underbrace{0, h, 2h, \cdots, 1-2h, 1-h, 1}_{n+1 \text{ element boundaries}}, \underbrace{1+h, \cdots, 1+ph}_{p \text{ terms}}\}. \tag{3.42}$$

The former knot vector is chosen such that the basis becomes interpolatory at the domain boundaries to facilitate the application of Dirichlet boundary conditions:

$$\hat{N}_0^p(0) = 1, \qquad \hat{N}_i^p(0) = 0 \quad \forall \, i \in \{1, \cdots, n+p-1\}, \tag{3.43}$$

$$\hat{N}_{n+p-1}^p(1) = 1, \quad \hat{N}_i^p(1) = 0 \quad \forall \, i \in \{0, \cdots, n+p-2\}. \tag{3.44}$$

Another property which is in particular import for the construction of the discrete finite element spaces is that the derivative of a B-spline is given by

$$\frac{\mathrm{d}\hat{N}_i^p}{\mathrm{d}\eta} = \frac{p}{\eta_{i+p} - \eta_i}\hat{N}_i^{p-1} - \frac{p}{\eta_{i+p+1} - \eta_{i+1}}\hat{N}_{i+1}^{p-1} := \hat{D}_{i-1}^{p-1} - \hat{D}_i^{p-1}, \tag{3.45}$$

where we defined scaled splines of one degree less which we call *D-splines*[4]. Note that $\hat{D}^{p-1}_{-1} = \hat{D}^{p-1}_{n+p-1} = 0$ which is why we remove these two splines from the space of D-splines. Furthermore, in case of periodic splines, we relate the last p (resp. $p-1$ in case of the D-splines) splines to the first p (resp. $p-1$) splines to ensure periodicity. Hence the number of *distinct* B-splines and D-splines, denoted by $\hat{n}_N$ and $\hat{n}_D$, respectively, reduces to

$$\text{clamped}: \quad \hat{n}_N = n + p \quad \hat{n}_D = \hat{n}_N - 1, \tag{3.46}$$

$$\text{periodic}: \quad \hat{n}_N = n \qquad \hat{n}_D = \hat{n}_N. \tag{3.47}$$

Using (3.45), the derivative of a finite element field f_h expanded in a B-splines basis can be written as

$$f_h(\eta) = \sum_{i=0}^{\hat{n}_N-1} f_i \hat{N}^p_i(\eta), \tag{3.48}$$

$$\Rightarrow \quad \frac{\mathrm{d}f_h}{\mathrm{d}\eta} = \sum_{i=0}^{\hat{n}_N-1} f_i \frac{\mathrm{d}\hat{N}^p_i}{\mathrm{d}\eta} = \sum_{i=0}^{\hat{n}_N-1} f_i(\hat{D}^{p-1}_{i-1} - \hat{D}^{p-1}_i) = \sum_{i=0}^{\hat{n}_D-1} (f_{i+1} - f_i)\hat{D}^{p-1}_i =: \sum_{i=0}^{\hat{n}_D-1} (\hat{\mathbb{G}}\mathbf{f})_i \hat{D}^{p-1}_i. \tag{3.49}$$

where $\mathbf{f} = (f_i)_{0\le i<\hat{n}_N}$ and $\hat{\mathbb{G}} \in \mathbb{R}^{\hat{n}_D\times\hat{n}_N}$ is the discrete gradient matrix

$$\hat{\mathbb{G}} := \underbrace{\begin{pmatrix} -1 & 1 & & & & \\ & -1 & 1 & & & \\ & & \ddots & \ddots & & \\ & & & -1 & 1 & \\ & & & & -1 & 1 \end{pmatrix}}_{\text{clamped}}, \qquad \hat{\mathbb{G}} := \underbrace{\begin{pmatrix} -1 & 1 & & & \\ & -1 & 1 & & \\ & & \ddots & \ddots & \\ & & & -1 & 1 \\ 1 & & & & -1 \end{pmatrix}}_{\text{periodic}}. \tag{3.50}$$

Using above results for univariate splines, one can easily construct the discrete de Rham sequence in three dimensions by starting with a tensor-product B-spline basis for the space V_0, followed by successively applying $\hat{\nabla}$, $\hat{\nabla}\times$ and $\hat{\nabla}\cdot$. This results in the following basis functions, number of basis functions and indices[5], which we all already used in (3.4):

$$V_0\left\{\ \Lambda^0_i(\boldsymbol{\eta}) := \hat{N}^{p_1}_{i_1}(\eta_1)\hat{N}^{p_2}_{i_2}(\eta_2)\hat{N}^{p_3}_{i_3}(\eta_3), \qquad N^0 = \hat{n}^1_N\hat{n}^2_N\hat{n}^3_N, \quad i = \hat{n}^2_N\hat{n}^3_N i_1 + \hat{n}^3_N i_2 + i_3 \right. \tag{3.51a}$$

$$\Big\downarrow \hat{\nabla}$$

$$V_1\begin{cases} \Lambda^1_{1,i}(\boldsymbol{\eta}) := \hat{D}^{p_1-1}_{i_1}(\eta_1)\hat{N}^{p_2}_{i_2}(\eta_2)\hat{N}^{p_3}_{i_3}(\eta_3), & N^1_1 = \hat{n}^1_D\hat{n}^2_N\hat{n}^3_N, \quad i = \hat{n}^2_N\hat{n}^3_N i_1 + \hat{n}^3_N i_2 + i_3 \\ \Lambda^1_{2,i}(\boldsymbol{\eta}) := \hat{N}^{p_1}_{i_1}(\eta_1)\hat{D}^{p_2-1}_{i_2}(\eta_2)\hat{N}^{p_3}_{i_3}(\eta_3), & N^1_2 = \hat{n}^1_N\hat{n}^2_D\hat{n}^3_N, \quad i = \hat{n}^2_D\hat{n}^3_N i_1 + \hat{n}^3_N i_2 + i_3 \\ \Lambda^1_{3,i}(\boldsymbol{\eta}) := \hat{N}^{p_1}_{i_1}(\eta_1)\hat{N}^{p_2}_{i_2}(\eta_2)\hat{D}^{p_3-1}_{i_3}(\eta_3), & N^1_3 = \hat{n}^1_N\hat{n}^2_N\hat{n}^3_D, \quad i = \hat{n}^2_N\hat{n}^3_D i_1 + \hat{n}^3_D i_2 + i_3 \end{cases} \tag{3.51b}$$

$$\Big\downarrow \hat{\nabla}\times$$

$$V_2\begin{cases} \Lambda^2_{1,i}(\boldsymbol{\eta}) := \hat{N}^{p_1}_{i_1}(\eta_1)\hat{D}^{p_2-1}_{i_2}(\eta_2)\hat{D}^{p_3-1}_{i_3}(\eta_3), & N^2_1 = \hat{n}^1_N\hat{n}^2_D\hat{n}^3_D, \quad i = \hat{n}^2_D\hat{n}^3_D i_1 + \hat{n}^3_D i_2 + i_3 \\ \Lambda^2_{2,i}(\boldsymbol{\eta}) := \hat{D}^{p_1-1}_{i_1}(\eta_1)\hat{N}^{p_2}_{i_2}(\eta_2)\hat{D}^{p_3-1}_{i_3}(\eta_3), & N^2_2 = \hat{n}^1_D\hat{n}^2_N\hat{n}^3_D, \quad i = \hat{n}^2_N\hat{n}^3_D i_1 + \hat{n}^3_D i_2 + i_3 \\ \Lambda^2_{3,i}(\boldsymbol{\eta}) := \hat{D}^{p_1-1}_{i_1}(\eta_1)\hat{D}^{p_2-1}_{i_2}(\eta_2)\hat{N}^{p_3}_{i_3}(\eta_3), & N^2_3 = \hat{n}^1_D\hat{n}^2_D\hat{n}^3_N, \quad i = \hat{n}^2_D\hat{n}^3_N i_1 + \hat{n}^3_N i_2 + i_3 \end{cases} \tag{3.51c}$$

$$\Big\downarrow \hat{\nabla}\cdot$$

$$V_3\left\{\ \Lambda^3_i(\boldsymbol{\eta}) := \hat{D}^{p_1-1}_{i_1}(\eta_1)\hat{D}^{p_2-1}_{i_2}(\eta_2)\hat{D}^{p_3-1}_{i_3}(\eta_3), \quad N^3 = \hat{n}^1_D\hat{n}^2_D\hat{n}^3_D, \quad i = \hat{n}^2_D\hat{n}^3_D i_1 + \hat{n}^3_D i_2 + i_3 \right. \tag{3.51d}$$

with $i = (i_1, i_2, i_3)$ being a 3d multi-index and $\hat{n}^\mu_{N/D}$ for $\mu \in \{1,2,3\}$ denoting the number of the one-dimensional B/D-splines in the μ-th direction on the logical domain. The 3d discrete derivatives

[4] It is convenient to start the indexing of the D-splines with -1 instead of 0.

[5] We use a row-major ordering in multi-dimensional arrays.

defined in (3.52) are obtained by Kronecker products of the 1d discrete gradient matrix defined in (3.50) with identity matrices of suitable shape. This yields the block matrices

$$\mathbb{G} := \begin{pmatrix} \hat{\mathbb{G}}^1 \otimes \mathbb{I}_{\hat{n}_N^2} \otimes \mathbb{I}_{\hat{n}_N^3} \\ \mathbb{I}_{\hat{n}_N^1} \otimes \hat{\mathbb{G}}^2 \otimes \mathbb{I}_{\hat{n}_N^3} \\ \mathbb{I}_{\hat{n}_N^1} \otimes \mathbb{I}_{\hat{n}_N^2} \otimes \hat{\mathbb{G}}^3 \end{pmatrix}, \tag{3.52a}$$

$$\mathbb{C} := \begin{pmatrix} 0 & -\mathbb{I}_{\hat{n}_N^1} \otimes \mathbb{I}_{\hat{n}_D^2} \otimes \hat{\mathbb{G}}^3 & \mathbb{I}_{\hat{n}_N^1} \otimes \hat{\mathbb{G}}^2 \otimes \mathbb{I}_{\hat{n}_D^3} \\ \mathbb{I}_{\hat{n}_D^1} \otimes \mathbb{I}_{\hat{n}_N^2} \otimes \hat{\mathbb{G}}^3 & 0 & -\hat{\mathbb{G}}^1 \otimes \mathbb{I}_{\hat{n}_N^2} \otimes \mathbb{I}_{\hat{n}_D^3} \\ -\mathbb{I}_{\hat{n}_D^1} \otimes \hat{\mathbb{G}}^2 \otimes \mathbb{I}_{\hat{n}_N^3} & \hat{\mathbb{G}}^1 \otimes \mathbb{I}_{\hat{n}_D^2} \otimes \mathbb{I}_{\hat{n}_N^3} & 0 \end{pmatrix}, \tag{3.52b}$$

$$\mathbb{D} := \begin{pmatrix} \hat{\mathbb{G}}^1 \otimes \mathbb{I}_{\hat{n}_D^2} \otimes \mathbb{I}_{\hat{n}_D^3} & \mathbb{I}_{\hat{n}_D^1} \otimes \hat{\mathbb{G}}^2 \otimes \mathbb{I}_{\hat{n}_D^3} & \mathbb{I}_{\hat{n}_D^1} \otimes \mathbb{I}_{\hat{n}_D^2} \otimes \hat{\mathbb{G}}^3 \end{pmatrix}. \tag{3.52c}$$

It can easily be verified that $\mathbb{C}\mathbb{G} = 0$ and $\mathbb{D}\mathbb{C} = 0$.

3.4.2 Commuting projectors

To ensure the commutativity of the diagram shown in Figure 1, we start from a one-dimensional quasi-interpolation method denoted by I^p onto the family of univariate B-splines of degree p defined by (3.40) and construct the corresponding commuting projector H^{p-1} according to

$$H^{p-1}f := \frac{\mathrm{d}}{\mathrm{d}\eta} I^p \left[\eta \mapsto \int_\tau^\eta f(t)\mathrm{d}t\right], \tag{3.53}$$

for some continuous function $f \in C([0,1])$. It is easily verified that $\mathrm{d}(I^p f)/\mathrm{d}\eta = H^{p-1}(\mathrm{d}f/\mathrm{d}\eta)$. The lower integration boundary τ can be chosen arbitrarily. The 3d projection operators are then constructed similarly to the basis functions (3.51) and discrete derivatives (3.52) by tensor-product considerations from the 1d operators. Note that the method explained hereafter is a rather special case of more general quasi spline interpolation techniques with the following properties [13]:

1. $I^p f$ is *local* in the sense that the value of $I^p f$ at η depends only on the values of f in a somewhat close vicinity to η.
2. I^p reproduces polynomials: $I^p(\eta^\gamma) = \eta^\gamma$ for $|\gamma| < p$.
3. $|I^p f - f| = \mathcal{O}(|h|^{p+1})$.

The motivation for our choice is in particular the locality of the method (first point) since this has the consequence that all matrices involving projections (e.g. (3.11)) are sparse which would not be the case if we chose a global interpolation method.

Given a knot vector $\hat{T} = \{\eta_i\}_{0\leq i\leq n+2p}$, we perform the following steps to obtain the i-th coefficient $\lambda_i(f)$ of the quasi-interpolant

$$I^p f = \sum_{i=0}^{\hat{n}_N - 1} \lambda_i(f)\hat{N}_i^p : \tag{3.54}$$

1. Choose $2p-1$ equidistant interpolation points $\{x_j^i\}_{0\leq j<2p-1}$ in the sub-interval $Q = [\eta_\mu, \eta_\nu]$ given by

$$\text{clamped}: \quad Q := \begin{cases} [\eta_p, \eta_{2p-1}], & i < p-1, \\ [\eta_{i+1}, \eta_{i+p}], & p-1 \leq i \leq \hat{n}_N - p, \\ [\eta_{\hat{n}_N - p+1}, \eta_{\hat{n}_N}], & i > \hat{n}_N - p, \end{cases} \tag{3.55}$$

$$\text{periodic}: \quad Q := \quad [\eta_{i+1}, \eta_{i+p}], \qquad \forall\, i. \tag{3.56}$$

2. Construct a local interpolant $I^Q f$ by solving the linear system

$$I^Q f(x_j^i) := \sum_{k=\mu-p}^{\nu-1} f_k \hat{N}_k^p(x_j^i) = f(x_j^i) \quad \forall\, j \in \{0, \cdots, 2p-2\}. \tag{3.57}$$

3. Set $\lambda_i(f) = f_i$.

Solving (3.57) means that the i-th global coefficient can be written as a linear combination of function values at the interpolation points

$$\lambda_i(f) = \sum_{j=0}^{2p-2} \omega_j^i f(x_j^i), \tag{3.58}$$

where the weights $\omega^i = \{\omega_j^i\}_{0\leq j<2p-1}$ form the line of the inverse collocation matrix with entries $\hat{N}_k^p(x_j^i)$ corresponding the coefficient f_i. The resulting weights are shown in Table 3 in Appendix C for generic quadratic and cubic B-splines. In practice, we store the weights and use (3.58) to compute the coefficients of the quasi-interpolant (3.54).

Using (3.53), the corresponding commuting projector $H^{p-1}f$ can be derived in the following way:

$$\begin{aligned} H^{p-1}f &= \frac{\mathrm{d}}{\mathrm{d}\eta}\left[\sum_i \lambda_i\left(\eta \mapsto \int_\tau^\eta f(t)\,\mathrm{d}t\right)\hat{N}_i^p\right] \\ &= -\sum_{i,j}\omega_j^i \int_{x_j^i}^\tau f(t)\,\mathrm{d}t \frac{\mathrm{d}\hat{N}_i^p}{\mathrm{d}\eta} \\ &= \sum_i\left[\sum_j\left(\omega_j^i \int_{x_j^i}^\tau f(t)\,\mathrm{d}t - \omega_j^{i+1}\int_{x_j^{i+1}}^\tau f(t)\,\mathrm{d}t\right)\right]\hat{D}_i^{p-1} \\ &=: \sum_i \tilde{\lambda}_i(f)\hat{D}_i^{p-1} \end{aligned} \tag{3.59}$$

From the second to the third line we used the fact that the derivative of a B-spline is equal to the difference of two neighboring D-splines (in the same way as in (3.49)). If we define $2p+1$ integration boundaries

$$\text{clamped}: \quad \tilde{x}^i := \begin{cases} x^{p-1} \cup x^p, & i < p-1, \\ x^i \cup x^{i+1}, & p-1 \leq i \leq \hat{n}_D - p, \\ x^{\hat{n}_D - p} \cup x^{\hat{n}_D - p+1}, & i > \hat{n}_D - p, \end{cases} \tag{3.60}$$

$$\text{periodic}: \quad \tilde{x}^i := \quad x^i \cup x^{i+1}, \qquad \forall\, i, \tag{3.61}$$

set $\tau = x_{2p-2}^{i+1}$ and split the integrals into integrals between two neighboring interpolation points, it is straightforward to show that the i-th coefficient can be computed as

$$\tilde{\lambda}_i(f) = \sum_{j=0}^{2p-1} \tilde{\omega}_j^i \int_{\tilde{x}_j^i}^{\tilde{x}_{j+1}^i} f(t)\,\mathrm{d}t, \tag{3.62}$$

with new weights given in Table 4 once more for generic degrees two and three[6]. We compute the integrals using $n_{\mathrm{q,pr}} > p$ Gauss-Legendre quadrature points and weights per integration interval.

The three-dimensional projectors $\Pi_0, \cdots, \Pi_3$ can now be constructed via compositions of the 1d

[6]Note that we always refer to the degree of the B-splines. Of course, if e.g. $p = 3$, we have quadratic D-splines.

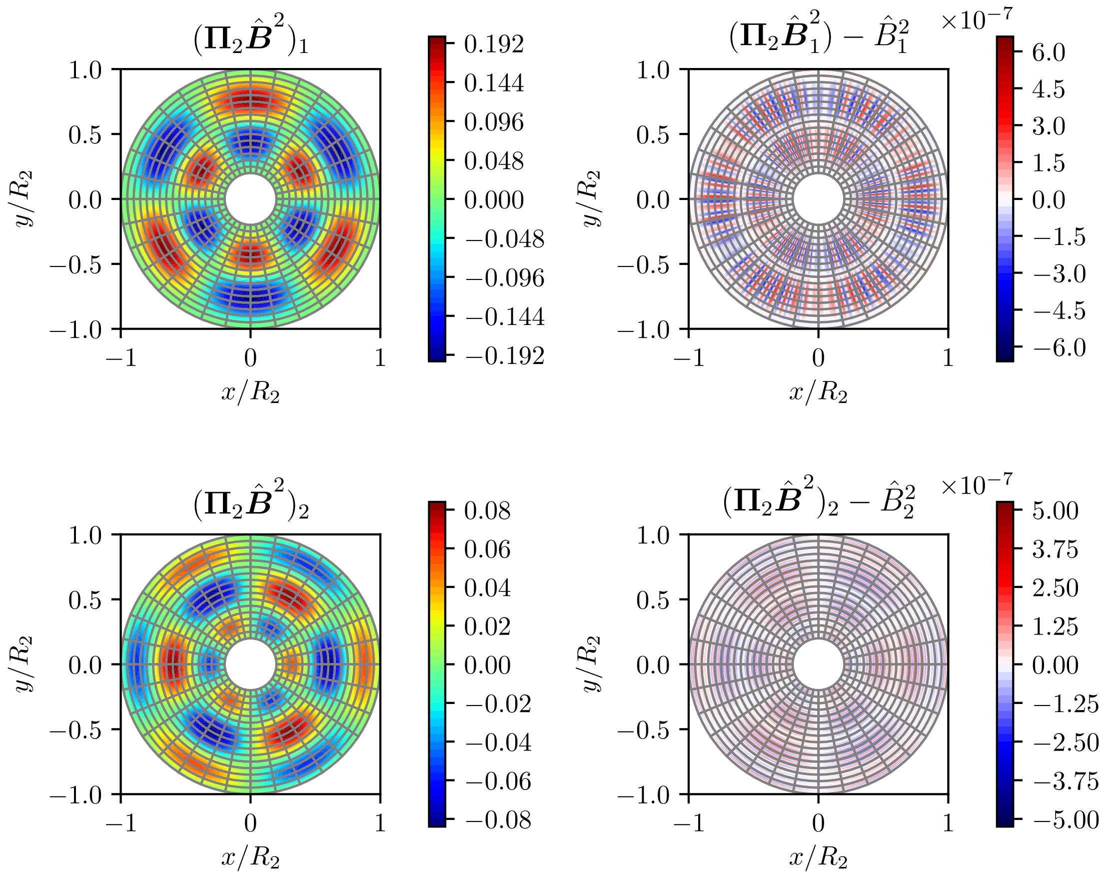

Figure 2: Projection of the components (3.65) using the projector (3.63c) on an annulus defined by the mapping (3.64) obtained with B-splines of degree $p = (3, 3, 1)$. The number of elements $N_{\mathrm{el}} = (128, 256, 2)$, number of quadrature points per integration interval $n_{\mathrm{q,pr}} = (4, 2, 2)$ and number of quadrature points per element for the computation of (3.66) $n_{\mathrm{q,el}} = (4, 2, 2)$. Top: contour plots at $z = 0.5L_z$ of the numerical 1-component (left) and error (right). Bottom: contour plots at $z = 0.5L_z$ of the numerical 2-component (left) and error (right).

operators I^p and H^{p-1}, respectively:

$$\Pi_0 = \quad I^{p_1} \odot I^{p_2} \odot I^{p_3} \quad = \quad I^{p_1}(\eta_1 \mapsto I^{p_2}(\eta_2 \mapsto I^{p_3}(\eta_3 \mapsto f(\eta_1, \eta_2, \eta_3)))), \tag{3.63a}$$

$$\boldsymbol{\Pi}_1 = \begin{pmatrix} H^{p_1-1} \odot I^{p_2} \odot I^{p_3} \\ I^{p_1} \odot H^{p_2-1} \odot I^{p_3} \\ I^{p_1} \odot I^{p_2} \odot H^{p_3-1} \end{pmatrix}, \tag{3.63b}$$

$$\boldsymbol{\Pi}_2 = \begin{pmatrix} I^{p_1} \odot H^{p_2-1} \odot H^{p_3-1} \\ H^{p_1-1} \odot I^{p_2} \odot H^{p_3-1} \\ H^{p_1-1} \odot H^{p_2-1} \odot I^{p_3} \end{pmatrix}, \tag{3.63c}$$

$$\Pi_3 = \quad H^{p_1-1} \odot H^{p_2-1} \odot H^{p_3-1}. \tag{3.63d}$$

As an example, we project the components of a given 2-form $\hat{\boldsymbol{B}}^2$ satisfying $\hat{\nabla} \cdot \hat{\boldsymbol{B}}^2 = 0$. For the geometry, we choose an annulus in the xy-plane with inner radius R_1 and outer radius R_2, such that $\Delta R = R_2 - R_1$. For completeness, we prescribe an extent of length L_z in z-direction. This geometry can be described by the mapping

$$\boldsymbol{F} : \hat{\Omega} \to \Omega, \quad \boldsymbol{\eta} \mapsto \begin{pmatrix} (R_1 + \eta_1 \Delta R)\cos(2\pi\eta_2) \\ (R_1 + \eta_1 \Delta R)\sin(2\pi\eta_2) \\ L_z \eta_3 \end{pmatrix} = \begin{pmatrix} x \\ y \\ z \end{pmatrix}. \tag{3.64}$$

We choose the components

$$\hat{\boldsymbol{B}}^2(\boldsymbol{\eta}) = \begin{pmatrix} \eta_1(1-\eta_1)\sin(2\pi\eta_1)\sin(6\pi\eta_2) \\ \frac{1}{6\pi}(1-2\eta_1)\sin(2\pi\eta_1) + \eta_1(1-\eta_1)\cos(2\pi\eta_1)2\pi]\cos(6\pi\eta_2) \\ 0 \end{pmatrix}, \tag{3.65}$$

clamped B-splines for the radial-like coordinate η_1 and periodic B-splines for the angle-like coordinate η_2 as well as for η_3. We measure the error of the projected components compared to the exact ones in the L^2-norm of the space of 2-forms,

$$||\Delta\hat{\boldsymbol{B}}^2||_{L^2} := ||\hat{\boldsymbol{B}}^2 - \boldsymbol{\Pi}_2\hat{\boldsymbol{B}}^2||_{L^2} = \int_{\hat{\Omega}} (\hat{\boldsymbol{B}}^2 - \boldsymbol{\Pi}_2\hat{\boldsymbol{B}}^2)^\top G(\hat{\boldsymbol{B}}^2 - \boldsymbol{\Pi}_2\hat{\boldsymbol{B}}^2)\frac{1}{\sqrt{g}}\,\mathrm{d}^3\eta, \tag{3.66}$$

as we refine the mesh (that is, as we increase the number of elements), computed using Gauss-Legendre quadrature points. Furthermore, to verify the commuting diagram property, we estimate the spatial L^∞-norm of $\hat{\nabla}\cdot\boldsymbol{\Pi}_2\hat{\boldsymbol{B}}^2$,

$$||\hat{\nabla}\cdot\boldsymbol{\Pi}_2\hat{\boldsymbol{B}}^2||_{L^\infty} := \max_{(\eta_1,\eta_2,\eta_3)\in\hat{\Omega}} |\hat{\nabla}\cdot\boldsymbol{\Pi}_2\hat{\boldsymbol{B}}^2|, \tag{3.67}$$

at the Greville points [15]. The resulting projected components are shown in Figure 2 for typical parameters. Table 1 shows the convergence of the projector while increasing the number of elements using quadratic and cubic splines. It can be seen that the divergence of the projected field is close to zero ($\approx 10^{-13}$= for any spline degree and resolution. This shows that the commuting diagram property is satisfied exactly.

	$p=(2,2,1)$			$p=(3,3,1)$		
N_{el}	$\|\|\Delta\hat{\boldsymbol{B}}^2\|\|_{L^2}$	Order	$\|\|\hat{\nabla}\cdot\boldsymbol{\Pi}_2\hat{\boldsymbol{B}}^2\|\|_{L^\infty}$	$\|\|\Delta\hat{\boldsymbol{B}}^2\|\|_{L^2}$	Order	$\|\|\hat{\nabla}\cdot\boldsymbol{\Pi}_2\hat{\boldsymbol{B}}^2\|\|_{L^\infty}$
$(32,64,2)$	$2.75\cdot10^{-4}$		$4.23\cdot10^{-12}$	$1.50\cdot10^{-5}$		$3.19\cdot10^{-14}$
$(64,128,2)$	$6.81\cdot10^{-5}$	2.01	$8.42\cdot10^{-14}$	$1.56\cdot10^{-6}$	3.27	$6.02\cdot10^{-14}$
$(128,256,2)$	$1.70\cdot10^{-5}$	2.00	$4.97\cdot10^{-14}$	$1.82\cdot10^{-7}$	3.10	$8.19\cdot10^{-14}$
$(256,512,2)$	$4.25\cdot10^{-6}$	2.00	$1.54\cdot10^{-13}$	$2.21\cdot10^{-8}$	3.04	$2.76\cdot10^{-13}$
$(512,1024,2)$	$1.06\cdot10^{-6}$	2.00	$3.42\cdot10^{-13}$	$2.73\cdot10^{-9}$	3.02	$5.86\cdot10^{-13}$

Table 1: Projection of the components (3.65) using the projector (3.63c) on an annulus defined by the mapping (3.64): p-th order convergence of the projector and divergence close to machine precision.

3.5 PIC coupling terms

We solve the Vlasov equation (2.6b) with classical particle-in-cell techniques. Hence we assume a particle-like distribution function which, in physical space Ω, takes the form

$$f_{\mathrm{h}} = f_{\mathrm{h}}(t,\boldsymbol{x},\boldsymbol{v}) \approx \sum_{k=1}^{K} w_k\delta(\boldsymbol{x}-\boldsymbol{x}_k(t))\delta(\boldsymbol{v}-\boldsymbol{v}_k(t)), \tag{3.68}$$

where K is the total number of simulation markers (to which we simply refer to as particles), w_k is the weight of the k-th particle and $\boldsymbol{x}_k=\boldsymbol{x}_k(t)$ and $\boldsymbol{v}_k=\boldsymbol{v}_k(t)$ its position in phase space at time t satisfying the equations of motion

$$\frac{\mathrm{d}\boldsymbol{x}_k}{\mathrm{d}t} = \boldsymbol{v}_k, \qquad \boldsymbol{x}_k(t=0)=\boldsymbol{x}_k^0, \tag{3.69a}$$

$$\frac{\mathrm{d}\boldsymbol{v}_k}{\mathrm{d}t} = \boldsymbol{B}(\boldsymbol{x}_k)\times\tilde{\boldsymbol{U}}(\boldsymbol{x}_k) + \boldsymbol{v}_k\times\boldsymbol{B}(\boldsymbol{x}_k), \qquad \boldsymbol{v}_k(t=0)=\boldsymbol{v}_k^0. \tag{3.69b}$$

To transform the equations of motion (3.69) to logical spatial coordinates $\boldsymbol{\eta}_k$, we note that $\mathrm{d}\boldsymbol{x}(\boldsymbol{\eta}(t))/\mathrm{d}t = DF\mathrm{d}\boldsymbol{\eta}/\mathrm{d}t$ for the first equation. Regarding the second equation, we first write it in curvilinear coordinates ($\boldsymbol{B} = DF\hat{\boldsymbol{B}}_\mathrm{f}$ and $\tilde{\boldsymbol{U}} = DF\hat{\boldsymbol{U}}$) and then use the relations (2.13) to transform the components $\hat{\boldsymbol{B}}_\mathrm{f}$ and $\hat{\boldsymbol{U}}$ the corresponding 2-form and 1-form components, respectively. Finally, we replace the continuous forms by their finite element approximations to obtain

$$\frac{\mathrm{d}\boldsymbol{\eta}_k}{\mathrm{d}t} = DF^{-1}(\boldsymbol{\eta}_k)\boldsymbol{v}_k, \tag{3.70a}$$

$$\frac{\mathrm{d}\boldsymbol{v}_k}{\mathrm{d}t} = (DF^{-1}(\boldsymbol{\eta}_k))^\top \left[\hat{\boldsymbol{B}}^2_{\mathrm{f}h}(\boldsymbol{\eta}_k) \times G^{-1}(\boldsymbol{\eta}_k)\hat{\boldsymbol{U}}^1_h(\boldsymbol{\eta}_k) - \hat{\boldsymbol{B}}^2_{\mathrm{f}h}(\boldsymbol{\eta}_k) \times DF^{-1}(\boldsymbol{\eta}_k)\boldsymbol{v}_k\right]. \tag{3.70b}$$

Here, we once more used the identity $M\boldsymbol{b} \times M\boldsymbol{c} = \det(M)(M^{-1})^\top(\boldsymbol{b}\times\boldsymbol{c})$.

We now turn our attention to the two terms $\mathrm{CC}(\rho_\mathrm{h})$ and $\mathrm{CC}(\boldsymbol{J}_\mathrm{h})$ in the weak momentum balance equation (3.20) involving the hot charge and current density. Following classical PIC techniques, the resulting integrals are evaluated by Monte-Carlo estimates using the particle positions in phase space [4]. Explicitly,

$$\mathrm{CC}(\rho_\mathrm{h}) \approx \int_{\hat{\Omega}} (\hat{\boldsymbol{C}}^1_h)^\top G^{-1}\hat{\rho}_\mathrm{h}\left(\hat{\boldsymbol{B}}^2_{\mathrm{f}h} \times G^{-1}\hat{\boldsymbol{U}}^1_h\right)\sqrt{g}\,\mathrm{d}^3\eta \tag{3.71}$$

$$= \int_{\hat{\Omega}}\int_{\mathbb{R}^3}\left\{(\hat{\boldsymbol{C}}^1_h)^\top G^{-1}\frac{\hat{f}_\mathrm{h}}{\hat{s}_\mathrm{h}}\left(\hat{\boldsymbol{B}}^2_{\mathrm{f}h} \times G^{-1}\hat{\boldsymbol{U}}^1_h\right)\right\}\hat{s}_\mathrm{h}\sqrt{g}\,\mathrm{d}^3v\,\mathrm{d}^3\eta \tag{3.72}$$

$$\approx \sum_{k=1}^{K} \underbrace{\frac{1}{K}\frac{\hat{f}^0_\mathrm{h}(\boldsymbol{\eta}^0_k,\boldsymbol{v}^0_k)}{\hat{s}^0_\mathrm{h}(\boldsymbol{\eta}^0_k,\boldsymbol{v}^0_k)}}_{=:w_k}(\hat{\boldsymbol{C}}^1_h)^\top(\boldsymbol{\eta}_k)G^{-1}(\boldsymbol{\eta}_k)\left(\hat{\boldsymbol{B}}^2_{\mathrm{f}h}(\boldsymbol{\eta}_k) \times G^{-1}(\boldsymbol{\eta}_k)\hat{\boldsymbol{U}}^1_h(\boldsymbol{\eta}_k)\right), \tag{3.73}$$

where we introduced the probability density function (PDF) $\hat{s}_\mathrm{h} = \hat{s}_\mathrm{h}(t,\boldsymbol{\eta},\boldsymbol{v}) = s_\mathrm{h}(t,\boldsymbol{F}(\boldsymbol{\eta}),\boldsymbol{v})$, which must be normalized to one and from which we demand to satisfy the Vlasov equation. Regarding the former, it is important to note that

$$1 = \int_\Omega\int_{\mathbb{R}^3} s_\mathrm{h}(t,\boldsymbol{x},\boldsymbol{v})\,\mathrm{d}^3x\,\mathrm{d}^3v = \int_{\hat{\Omega}}\int_{\mathbb{R}^3}\hat{s}_\mathrm{h}(t,\boldsymbol{\eta},\boldsymbol{v})\sqrt{g}(\boldsymbol{\eta})\,\mathrm{d}^3\eta\,\mathrm{d}^3v, \qquad \forall\, t\in\mathbb{R}^+_0, \tag{3.74}$$

such that the transformed PDF is given by $\tilde{s}_\mathrm{h} := \hat{s}_\mathrm{h}\sqrt{g}$. Then (3.72) can be interpreted as the expectation value of the random variable inside the curly brackets distributed under the PDF $\tilde{s}_\mathrm{h}$ with (3.73) being its estimator using the particle positions $(\boldsymbol{\eta}_k,\boldsymbol{v}_k)_{1\leq k\leq N_\mathrm{p}}$ in phase space. Finally, we made use of the fact that $\hat{f}_\mathrm{h}$ and $\hat{s}_\mathrm{h}$ are constant along a particle trajectory according to the Vlasov equation, that is, $\mathrm{d}\hat{f}_\mathrm{h}/\mathrm{d}t = 0$ in a Lagrangian frame, i.e. $\hat{f}_\mathrm{h}(t,\boldsymbol{\eta}_k(t),\boldsymbol{v}_k(t)) = \hat{f}^0_\mathrm{h}(\boldsymbol{\eta}^0_k,\boldsymbol{v}^0_k)$, where $\hat{f}^0_\mathrm{h} = \hat{f}_\mathrm{h}(t=0,\boldsymbol{\eta},\boldsymbol{v}) = f_\mathrm{h}(t=0,\boldsymbol{F}(\boldsymbol{\eta}),\boldsymbol{v})$ denotes the initial distribution function and $(\boldsymbol{\eta}^0_k,\boldsymbol{v}^0_k)$ is the initial position of the k-th particle in phase space drawn from the initial PDF $\hat{s}^0_\mathrm{h}$. Hence the particle weights $(w_k)_{1\leq k\leq N_\mathrm{p}}$ are constant in time which is not the case if, as shown in Appendix B, a δf approach is used. One should keep in mind that if one samples from the transformed PDF $\tilde{s}_\mathrm{h}$, one must not forget the Jacobian determinant in the definition of the weights.

In order to write (3.73) as well as (3.70) in matrix-vector form, we introduce the following vectors and matrices:

- $\boldsymbol{H} := (\eta_{1,1},\cdots,\eta_{K,1},\eta_{1,2},\cdots,\eta_{K,2},\eta_{1,3},\cdots,\eta_{K,3})^\top \in \mathbb{R}^{3K}$,
- $\boldsymbol{V} := (v_{1,x},\cdots,v_{K,x},v_{1,y},\cdots,v_{K,y},v_{1,z},\cdots,v_{K,z})^\top \in \mathbb{R}^{3K}$,
- $\mathbb{W} := \mathbb{I}_3 \otimes \mathrm{diag}(w_1,\cdots,w_K) \in \mathbb{R}^{3K\times 3K}$,
- $\mathbb{P}^n_\mu(\boldsymbol{H}) := (\Lambda^n_{\mu,i}(\boldsymbol{\eta}_k))_{0\leq i\leq N^n_\mu-1,1\leq k\leq K}$ $\quad (n\in\{1,2\},\ \mu\in\{1,2,3\})$ $\quad \in \mathbb{R}^{N^n_\mu\times K}$,
- $\mathbb{P}^n(\boldsymbol{H}) := \mathrm{diag}(\mathbb{P}^n_1,\ \mathbb{P}^n_2,\ \mathbb{P}^n_3)$ $\quad (n\in\{1,2\})$ $\quad \in \mathbb{R}^{N^n\times 3K}$,
- $\bar{G}^{-1}_{ab}(\boldsymbol{H}) := \mathrm{diag}(G^{-1}_{ab}(\boldsymbol{\eta}_1),\cdots,G^{-1}_{ab}(\boldsymbol{\eta}_K))$ $\quad (a,b\in\{1,2,3\})$ $\quad \in \mathbb{R}^{K\times K}$,

- $\bar{G}^{-1}(\boldsymbol{H}) \quad := (\bar{G}^{-1}_{ab})_{1\leq a,b\leq 3} \qquad \in \mathbb{R}^{3K\times 3K}$,
- $\bar{DF}^{-1}_{ab}(\boldsymbol{H}) := \mathrm{diag}(DF^{-1}_{ab}(\boldsymbol{\eta}_1), \cdots, DF^{-1}_{ab}(\boldsymbol{\eta}_K)) \quad (a,b \in \{1,2,3\}) \qquad \in \mathbb{R}^{K\times K}$,
- $\bar{DF}^{-1}(\boldsymbol{H}) := (\bar{DF}^{-1}_{ab})_{1\leq a,b\leq 3} \qquad \in \mathbb{R}^{3K\times 3K}$,
- $\mathbb{B}_{\mathrm{f},\mu}(\mathbf{b}, \boldsymbol{H}) := \mathrm{diag}(\mathbf{b}_\mu^\top \mathbb{P}^2_\mu) + \mathrm{diag}(\hat{B}_{\mathrm{eq},\mu}(\boldsymbol{\eta}_1), \cdots, \hat{B}_{\mathrm{eq},\mu}(\boldsymbol{\eta}_K)) \quad \mu \in \{1,2,3\} \qquad \in \mathbb{R}^{K\times K}$,

where $\mathbb{I}_3 \in \mathbb{R}^{3\times 3}$ denotes the three-dimensional identity matrix and $\otimes$ the Kronecker product. In accordance with (3.16), we additionally define the block matrix

$$\mathbb{B}_{\mathrm{f}} = \mathbb{B}_{\mathrm{f}}(\mathbf{b}, \boldsymbol{H}) := \begin{pmatrix} 0 & -\mathbb{B}_{\mathrm{f},3} & \mathbb{B}_{\mathrm{f},2} \\ \mathbb{B}_{\mathrm{f},3} & 0 & -\mathbb{B}_{\mathrm{f},1} \\ -\mathbb{B}_{\mathrm{f},2} & \mathbb{B}_{\mathrm{f},1} & 0 \end{pmatrix} \in \mathbb{R}^{3K\times 3NK}, \tag{3.75}$$

which represents the cross product with the total magnetic field at all particle positions. With this (3.73) becomes

$$\mathrm{CC}(\rho_{\mathrm{ch}}) \approx \mathbf{c}^\top \mathbb{P}^1 \mathbb{W} \bar{G}^{-1} \mathbb{B}_{\mathrm{f}} \bar{G}^{-1} (\mathbb{P}^1)^\top \mathbf{u}. \tag{3.76}$$

The same procedure holds for the term involving the hot current density:

$$\begin{aligned}
\mathrm{CC}(\boldsymbol{J}_{\mathrm{h}}) &\approx \int_{\hat{\Omega}} (\hat{\boldsymbol{C}}^1_h)^\top G^{-1} \left(\hat{\boldsymbol{B}}^2_{\mathrm{f}h} \times \hat{\boldsymbol{J}}_{\mathrm{h}} \right) \sqrt{g}\, \mathrm{d}^3\eta & (3.77)\\
&= \int_{\hat{\Omega}} \int_{\mathbb{R}^3} \left\{ (\hat{\boldsymbol{C}}^1_h)^\top G^{-1} \frac{\hat{f}_{\mathrm{h}}}{\hat{s}_{\mathrm{h}}} \left(\hat{\boldsymbol{B}}^2_{\mathrm{f}h} \times DF^{-1} \boldsymbol{v} \right) \right\} \hat{s}_{\mathrm{h}} \sqrt{g}\, \mathrm{d}^3 v\, \mathrm{d}^3\eta & (3.78)\\
&\approx \sum_{k=1}^{N_{\mathrm{p}}} w_k (\hat{\boldsymbol{C}}^1_h)^\top (\boldsymbol{\eta}_k) G^{-1}(\boldsymbol{\eta}_k) \left(\hat{\boldsymbol{B}}^2_{\mathrm{f}h}(\boldsymbol{\eta}_k) \times DF^{-1}(\boldsymbol{\eta}_k) \boldsymbol{v}_k \right) & (3.79)\\
&= \mathbf{c}^\top \mathbb{P}^1 \mathbb{W} \bar{G}^{-1} \mathbb{B}_{\mathrm{f}} \bar{DF}^{-1} \boldsymbol{V}. & (3.80)
\end{aligned}$$

Collecting the terms (3.27), (3.30), (3.29) and (3.28), we find in summary the following semi-discrete momentum balance equation:

$$\mathcal{A}\dot{\mathbf{u}} = \mathcal{T}^\top \mathbb{C}^\top \mathbb{M}^2 \mathbf{b} + \mathbb{M}^1 \mathcal{P} \mathbf{b} - \mathbb{P}^1 \mathbb{W} \bar{G}^{-1} \mathbb{B}_{\mathrm{f}} \bar{G}^{-1} (\mathbb{P}^1)^\top \mathbf{u} + \mathbb{P}^1 \mathbb{W} \bar{G}^{-1} \mathbb{B}_{\mathrm{f}} \bar{DF}^{-1} \boldsymbol{V} - \mathbb{M}^1 \mathbb{G} \mathbf{p}. \tag{3.81}$$

Finally, we also write the equations of motion (3.70) of all particles in a compact matrix-vector form:

$$\begin{aligned}
\frac{\mathrm{d}\boldsymbol{H}}{\mathrm{d}t} &= \bar{DF}^{-1}(\boldsymbol{H}) \boldsymbol{V}, & (3.82\mathrm{a})\\
\frac{\mathrm{d}\boldsymbol{V}}{\mathrm{d}t} &= (\bar{DF}^{-1}(\boldsymbol{H}))^\top \left[\mathbb{B}_{\mathrm{f}}(\mathbf{b}, \boldsymbol{H}) \bar{G}^{-1}(\boldsymbol{H}) (\mathbb{P}^1)^\top (\boldsymbol{H}) \mathbf{u} - \mathbb{B}_{\mathrm{f}}(\mathbf{b}, \boldsymbol{H}) \bar{DF}^{-1}(\boldsymbol{H}) \boldsymbol{V} \right]. & (3.82\mathrm{b})
\end{aligned}$$

3.6 Energy and Hamiltonian system

Let us define the discrete energy corresponding to (2.7). We use the same splitting (3.24) for the kinetic energy of the bulk plasma in order to end up with the same matrix $\mathcal{A}$ as in the semi-discrete momentum balance equation (3.81):

$$\begin{aligned}
\mathcal{H}_{1h} :&= \frac{1}{4} \int_{\hat{\Omega}} \left[\boldsymbol{\Pi}_1 \left(\frac{\hat{\rho}^3_{\mathrm{eq}}}{\sqrt{g}} \hat{\boldsymbol{U}}^1_h \right) \right]^\top G^{-1} \hat{\boldsymbol{U}}^1_h \sqrt{g}\, \mathrm{d}^3\eta + \frac{1}{4} \int_{\hat{\Omega}} \left(\hat{\boldsymbol{U}}^1_h \right)^\top G^{-1} \boldsymbol{\Pi}_1 \left(\frac{\hat{\rho}^3_{\mathrm{eq}}}{\sqrt{g}} \hat{\boldsymbol{U}}^1_h \right) \sqrt{g}\, \mathrm{d}^3\eta \\
&\quad + \frac{1}{2} \int_{\hat{\Omega}} (\hat{\boldsymbol{B}}^2_h)^\top G \hat{\boldsymbol{B}}^2_h \frac{1}{\sqrt{g}}\, \mathrm{d}^3\eta + \frac{1}{\gamma - 1} \int_{\hat{\Omega}} \hat{p}^0_h \sqrt{g}\, \mathrm{d}^3\eta + \frac{1}{2} \int_{\hat{\Omega}} \int_{\mathbb{R}^3} v^2 f_{\mathrm{h}}\, \mathrm{d}^3 v\, \mathrm{d}^3 x \qquad (3.83)\\
&= \frac{1}{2} \mathbf{u}^\top \mathcal{A} \mathbf{u} + \frac{1}{2} \mathbf{b}^\top \mathbb{M}^2 \mathbf{b} + \frac{1}{\gamma - 1} \mathbf{p}^\top \mathbf{n} + \frac{1}{2} \boldsymbol{V}^\top \mathbb{W} \boldsymbol{V}.
\end{aligned}$$

The expression for the energy of the kinetic species (last term) is simply obtained by using the discrete distribution function (3.68) and evaluating the integrals. The vector $\mathbf{n}$ contains all integrals of each basis function in V_0 over $\hat{\Omega}$, i.e.

$$\mathbf{n} := \left(\int_{\hat{\Omega}} \Lambda^0_0 \sqrt{g}\, \mathrm{d}^3\eta, \cdots, \int_{\hat{\Omega}} \Lambda^0_{N^0-1} \sqrt{g}\, \mathrm{d}^3\eta \right)^\top . \tag{3.84}$$

If we collect all finite element coefficients and particle positions in phase space in a single vector $\mathbf{R}^\top := (\boldsymbol{\rho}^\top, \mathbf{u}^\top, \mathbf{p}^\top, \mathbf{b}^\top, \boldsymbol{H}^\top, \boldsymbol{V}^\top) \in \mathbb{R}^{N^3+N^1+N^0+N^2+3N_\mathrm{p}+3N_\mathrm{p}}$, we can write the semi-discrete MHD equations (3.10), (3.15), (3.39) and (3.81) and PIC equations (3.82) in the following compact form:

$$\begin{aligned}\frac{\mathrm{d}\mathbf{R}}{\mathrm{d}t} = \mathbb{J}\nabla_{\mathbf{R}}\mathcal{H}_{1h} + \mathbb{K}\mathbf{R} = &\begin{pmatrix} 0 & 0 & 0 & 0 & 0 & 0 \\ 0 & \mathbb{J}_{11}(\mathbf{b},\boldsymbol{H}) & \mathbb{J}_{12} & 0 & 0 & \mathbb{J}_{14}(\mathbf{b},\boldsymbol{H}) \\ 0 & 0 & 0 & 0 & 0 & 0 \\ 0 & -\mathbb{J}_{12}^\top & 0 & 0 & 0 & 0 \\ 0 & 0 & 0 & 0 & 0 & \mathbb{J}_{34}(\boldsymbol{H}) \\ 0 & -\mathbb{J}_{14}^\top(\mathbf{b},\boldsymbol{H}) & 0 & 0 & -\mathbb{J}_{34}^\top(\boldsymbol{H}) & \mathbb{J}_{44}(\mathbf{b},\boldsymbol{H}) \end{pmatrix} \begin{pmatrix} 0 \\ \mathcal{A}\mathbf{u} \\ 0 \\ \mathbb{M}^2\mathbf{b} \\ 0 \\ \mathbb{W}\mathbf{V} \end{pmatrix} \\ &+ \begin{pmatrix} 0 & -\mathbb{D}\mathcal{Q} & 0 & 0 & 0 & 0 \\ 0 & 0 & \mathcal{A}^{-1}\mathbb{M}^1\mathcal{P} & -\mathcal{A}^{-1}\mathbb{M}^1\mathbb{G} & 0 & 0 \\ 0 & (\mathbb{M}^0)^{-1}\left[\mathbb{G}^\top\mathbb{M}^1\mathcal{S} + (\gamma-1)\mathcal{K}^\top\mathbb{G}^\top\mathbb{M}^1\right] & 0 & 0 & 0 & 0 \\ 0 & 0 & 0 & 0 & 0 & 0 \\ 0 & 0 & 0 & 0 & 0 & 0 \\ 0 & 0 & 0 & 0 & 0 & 0 \end{pmatrix} \begin{pmatrix} \boldsymbol{\rho} \\ \mathbf{u} \\ \mathbf{p} \\ \mathbf{b} \\ \boldsymbol{H} \\ \mathbf{V} \end{pmatrix}. \end{aligned} \tag{3.85}$$

We find that our spatial discretization results in a system which can be written as the sum of a non-canonical Hamiltonian part with the Poisson matrix $\mathbb{J}$ and a non-Hamiltonian part with the matrix $\mathbb{K}$. As already mentioned in Section 2, the latter only plays a role for compressible waves and if $\nabla \times \boldsymbol{B}_\mathrm{eq} \neq 0$ (then $\mathcal{P} = 0$). In particular, we remark that obtaining the Hamiltonian part relies on the symmetry of $\mathcal{A}$, $\mathbb{M}^2$ and $\mathbb{W}$. While it obvious for the last two matrices, the symmetry of $\mathcal{A}$ is ensured by the splitting performed in (3.24). In in this case the anti-symmetry of $\mathbb{J}$ immediately implies conservation of $\mathcal{H}_{1h}$. The single blocks of $\mathbb{J}$ are given by

$$\mathbb{J}_{11}(\mathbf{b},\boldsymbol{H}) = -\mathcal{A}^{-1}\mathbb{P}^1(\boldsymbol{H})\mathbb{W}\bar{G}^{-1}(\boldsymbol{H})\mathbb{B}_\mathrm{f}(\mathbf{b},\boldsymbol{H})\bar{G}^{-1}(\boldsymbol{H})(\mathbb{P}^1)^\top(\boldsymbol{H})\mathcal{A}^{-1}, \tag{3.86a}$$

$$\mathbb{J}_{12} = \mathcal{A}^{-1}\mathcal{T}^\top\mathbb{C}^\top, \tag{3.86b}$$

$$\mathbb{J}_{14}(\mathbf{b},\boldsymbol{H}) = \mathcal{A}^{-1}\mathbb{P}^1(\boldsymbol{H})\tilde{G}^{-1}(\boldsymbol{H})\mathbb{B}_\mathrm{f}(\mathbf{b},\boldsymbol{H})\tilde{DF}^{-1}(\boldsymbol{H}), \tag{3.86c}$$

$$\mathbb{J}_{34}(\boldsymbol{H}) = \bar{DF}^{-1}(\boldsymbol{H})\mathbb{W}^{-1}, \tag{3.86d}$$

$$\mathbb{J}_{44}(\mathbf{b},\boldsymbol{H}) = -(\tilde{DF}^{-1})^\top(\boldsymbol{H})\mathbb{B}_\mathrm{f}(\mathbf{b},\boldsymbol{H})\tilde{DF}^{-1}(\boldsymbol{H})\mathbb{W}^{-1}. \tag{3.86e}$$

4 Time discretization

In order to keep the energy conservation property, we propose two splitting steps: First, we split apart the non-Hamiltonian part $\mathbb{K}\mathbf{R}$, and second, we apply Poisson splitting to the Hamiltonian part $\mathbb{J}\nabla_{\mathbf{R}}\mathcal{H}_{1\mathrm{h}}$ and solve each (anti-symmetric) sub-step in an energy conserving way. We recall the Hamiltonian part:

$$\frac{\mathrm{d}}{\mathrm{d}t}\begin{pmatrix} \mathbf{u} \\ \mathbf{b} \\ \boldsymbol{H} \\ \boldsymbol{V} \end{pmatrix} = \begin{pmatrix} \mathbb{J}_{11}(\mathbf{b},\boldsymbol{H}) & \mathbb{J}_{12} & 0 & \mathbb{J}_{14}(\mathbf{b},\boldsymbol{H}) \\ -\mathbb{J}_{12}^\top & 0 & 0 & 0 \\ 0 & 0 & 0 & \mathbb{J}_{34}(\boldsymbol{H}) \\ -\mathbb{J}_{14}^\top(\mathbf{b},\boldsymbol{H}) & 0 & -\mathbb{J}_{34}^\top(\boldsymbol{H}) & \mathbb{J}_{44}(\mathbf{b},\boldsymbol{H}) \end{pmatrix} \begin{pmatrix} \mathcal{A}\mathbf{u} \\ \mathbb{M}^2\mathbf{b} \\ 0 \\ \mathbb{W}\boldsymbol{V} \end{pmatrix}. \tag{4.1}$$

Introducing a temporal grid $t_n = n\Delta t$ with $n \in \mathbb{N}_0$ yields to following sub-steps:

Sub-step 1 The first sub-system reads

$$\dot{\mathbf{u}} = \mathbb{J}_{11}(\mathbf{b}, \boldsymbol{H})\mathcal{A}\mathbf{u}, \qquad \dot{\mathbf{b}} = 0, \qquad \dot{\boldsymbol{H}} = 0, \qquad \dot{\boldsymbol{V}} = 0. \tag{4.2}$$

We solve the equation for $\mathbf{u}$ with the energy-preserving, implicit Crank-Nicolson method [12]. $\mathbb{J}_{11} = \mathbb{J}_{11}(\mathbf{b}^n, \boldsymbol{H}^n)$ remains constant in this step:

$$\mathbf{u}^{n+1} = \mathbf{u}^n + \frac{\Delta t}{2}\mathbb{J}_{11}(\mathbf{b}^n, \boldsymbol{H}^n)\mathcal{A}(\mathbf{u}^n + \mathbf{u}^{n+1}), \tag{4.3}$$

$$\Leftrightarrow \quad \left(\mathbb{I} - \frac{\Delta t}{2}\mathbb{J}_{11}(\mathbf{b}^n, \boldsymbol{H}^n)\mathcal{A}\right)\mathbf{u}^{n+1} = \left(\mathbb{I} + \frac{\Delta t}{2}\mathbb{J}_{11}(\mathbf{b}^n, \boldsymbol{H}^n)\mathcal{A}\right)\mathbf{u}^n. \tag{4.4}$$

To avoid multiple matrix inversions, we multiply the second line with $\mathcal{A}$ from the left-hand side to obtain

$$\left(\mathcal{A} - \frac{\Delta t}{2}\mathcal{A}\mathbb{J}_{11}(\mathbf{b}^n, \boldsymbol{H}^n)\mathcal{A}\right)\mathbf{u}^{n+1} = \left(\mathcal{A} + \frac{\Delta t}{2}\mathcal{A}\mathbb{J}_{11}(\mathbf{b}^n, \boldsymbol{H}^n)\mathcal{A}\right)\mathbf{u}^n. \tag{4.5}$$

We denote the corresponding integrator by $\Phi^1_{\Delta t} : \mathbb{R}^{N^1} \to \mathbb{R}^{N^1}$, $\mathbf{u}^n \mapsto \mathbf{u}^{n+1}$.

Sub-step 2 The second sub-system reads

$$\dot{\mathbf{u}} = \mathbb{J}_{12}\mathbb{M}^2\mathbf{b}, \qquad \dot{\mathbf{b}} = -\mathbb{J}_{12}^\top\mathcal{A}\mathbf{u}, \qquad \dot{\boldsymbol{H}} = 0, \qquad \dot{\boldsymbol{V}} = 0. \tag{4.6}$$

As before, we solve this system with the Crank-Nicolson method,

$$\mathbf{u}^{n+1} = \mathbf{u}^n + \frac{\Delta t}{2}\mathcal{A}^{-1}\mathcal{T}^\top\mathbb{C}^\top(\mathbf{b}^n + \mathbf{b}^{n+1}), \tag{4.7}$$

$$\mathbf{b}^{n+1} = \mathbf{b}^n - \frac{\Delta t}{2}\mathbb{C}\mathcal{T}\Delta t(\mathbf{u}^n + \mathbf{u}^{n+1}), \tag{4.8}$$

ans solve for $\mathbf{u}^{n+1}$ by plugging the second into the first equation. After some straightforward manipulations this results in

$$\mathbf{u}^{n+1} = S_2^{-1}\left[\left(\mathcal{A} - \frac{\Delta t^2}{4}\mathcal{T}^\top\mathbb{C}^\top\mathbb{M}^2\mathbb{C}\mathcal{T}\right)\mathbf{u}^n + \Delta t\mathcal{T}^\top\mathbb{C}^\top\mathbb{M}^2\mathbf{b}^n\right], \tag{4.9}$$

$$\mathbf{b}^{n+1} = \mathbf{b}^n - \frac{\Delta t}{2}\mathbb{C}\mathcal{T}(\mathbf{u}^n + \mathbf{u}^{n+1}), \tag{4.10}$$

where $S_2 := \mathcal{A} + \Delta t^2\mathcal{T}^\top\mathbb{C}^\top\mathbb{M}^2\mathbb{C}\mathcal{T}/4$. Particularly, we note the explicit update rule for $\mathbf{b}$ which preserves the divergence-free constraint, i.e. $\mathbb{D}\mathbf{b}^{n+1} = \mathbb{D}\mathbf{b}^n$ due to $\mathbb{D}\mathbb{C} = 0$. We denote the corresponding integrator by $\Phi^2_{\Delta t} : \mathbb{R}^{N^1} \times \mathbb{R}^{N^2} \to \mathbb{R}^{N^1} \times \mathbb{R}^{N^2}$, $\mathbf{u}^n, \mathbf{b}^n \mapsto \mathbf{u}^{n+1}, \mathbf{b}^{n+1}$.

Sub-step 3 The third sub-system reads

$$\dot{\mathbf{u}} = \mathbb{J}_{14}(\mathbf{b}, \boldsymbol{H})\mathbb{W}\boldsymbol{V}, \qquad \dot{\mathbf{b}} = 0, \qquad \dot{\boldsymbol{H}} = 0, \qquad \dot{\boldsymbol{V}} = -\mathbb{J}_{14}^\top(\mathbf{b}, \boldsymbol{H})\mathcal{A}\mathbf{u}. \tag{4.11}$$

We solve this system in the same way as before. Since $\mathbf{b}$ and $\boldsymbol{H}$ do not change in this step, the same is true for the matrix $\mathbb{J}_{14}$. Hence $\mathbb{J}_{14} = \mathbb{J}_{14}(\mathbf{b}^n, \boldsymbol{H}^n)$ and we have

$$\mathbf{u}^{n+1} = \mathbf{u}^n + \frac{\Delta t}{2}\mathbb{J}_{14}\mathbb{W}(\boldsymbol{V}^n + \boldsymbol{V}^{n+1}), \tag{4.12}$$

$$\boldsymbol{V}^{n+1} = \boldsymbol{V}^n - \frac{\Delta t}{2}\mathbb{J}_{14}^\top(\mathbf{u}^n + \mathbf{u}^{n+1}), \tag{4.13}$$

$$\Leftrightarrow \quad \mathbf{u}^{n+1} = S_3^{-1}\left[\left(\mathcal{A} - \frac{\Delta t^2}{4}\mathcal{A}\mathbb{J}_{14}\mathbb{W}\mathbb{J}_{14}^\top\mathcal{A}\right)\mathbf{u}^n + \Delta t\mathcal{A}\mathbb{J}_{14}\mathbb{W}\boldsymbol{V}^n\right], \tag{4.14}$$

$$\Leftrightarrow \quad \boldsymbol{V}^{n+1} = \boldsymbol{V}^n - \frac{\Delta t}{2}\mathbb{J}_{14}^\top\mathcal{A}(\mathbf{u}^n + \mathbf{u}^{n+1}), \tag{4.15}$$

where $S_3 := \mathcal{A} + \Delta t^2\mathcal{A}\mathbb{J}_{14}\mathbb{W}\mathbb{J}_{14}^\top\mathcal{A}/4$. We denote the corresponding integrator by $\Phi^3_{\Delta t} : \mathbb{R}^{N^1} \times \mathbb{R}^{3N_\mathrm{p}} \to \mathbb{R}^{N^1} \times \mathbb{R}^{3N_\mathrm{p}}$, $\mathbf{u}^n, \boldsymbol{V}^n \mapsto \mathbf{u}^{n+1}, \boldsymbol{V}^{n+1}$.

Sub-step 4 The fourth sub-system reads

$$\dot{\mathbf{u}} = 0, \qquad \dot{\mathbf{b}} = 0, \qquad \dot{\boldsymbol{H}} = \bar{DF}^{-1}(\boldsymbol{H})\boldsymbol{V}, \qquad \dot{\boldsymbol{V}} = 0. \tag{4.16}$$

Since this step does not play a role for conservation of energy (the discrete Hamiltonian does not depend on the particle spatial coordinates), we apply to this system a standard fourth order Runge-Kutta scheme and denote the integrator by $\Phi^4_{\Delta t} : \mathbb{R}^{3N_\mathrm{p}} \times \mathbb{R}^{3N_\mathrm{p}}$, $\boldsymbol{H}^n \mapsto \boldsymbol{H}^{n+1}$.

Sub-step 5 The fifth sub-system reads

$$\dot{\mathbf{u}} = 0, \qquad \dot{\mathbf{b}} = 0, \qquad \dot{\boldsymbol{H}} = 0, \qquad \dot{\boldsymbol{V}} = \mathbb{J}_{44}(\mathbf{b}, \boldsymbol{H})\mathbb{W}\mathbf{V}. \tag{4.17}$$

Using once more the Crank-Nicolson scheme yields

$$\begin{aligned} \left[\mathbb{I} + \frac{\Delta t}{2}(\bar{DF}^{-1}(\boldsymbol{H}^n))^\top \mathbb{B}_\mathrm{f}(\mathbf{b}^n, \boldsymbol{H}^n)\bar{DF}^{-1}(\boldsymbol{H}^n)\right] \boldsymbol{V}^{n+1} & \\ = \left[\mathbb{I} - \frac{\Delta t}{2}(\bar{DF}^{-1}(\boldsymbol{H}^n))^\top \mathbb{B}_\mathrm{f}(\mathbf{b}^n, \boldsymbol{H}^n)\bar{DF}^{-1}(\boldsymbol{H}^n)\right] \boldsymbol{V}^n & \end{aligned} \tag{4.18}$$

We denote the corresponding integrator by $\Phi^5_{\Delta t} : \mathbb{R}^{3N_\mathrm{p}} \times \mathbb{R}^{3N_\mathrm{p}}$, $\boldsymbol{V}^n \mapsto \boldsymbol{V}^{n+1}$.

Sub-step 6 (Non-Hamiltonian part) The sixth sub-system reads

$$\dot{\boldsymbol{\rho}} = -\mathbb{D}\mathcal{Q}\mathbf{u}, \qquad \mathcal{A}\dot{\mathbf{u}} = -\mathbb{M}^1\mathbb{G}\mathbf{p} + \mathbb{M}^1\mathcal{P}\mathbf{b}, \qquad \mathbb{M}^0\dot{\mathbf{p}} = \left[\mathbb{G}^\top\mathbb{M}^1\mathcal{S} + (\gamma-1)\mathcal{K}^\top\mathbb{G}^\top\mathbb{M}^1\right]\mathbf{u}, \qquad \dot{\mathbf{b}} = 0. \tag{4.19}$$

Defining $\mathbb{L} := \mathbb{G}^\top\mathbb{M}^1\mathcal{S} + (\gamma-1)\mathcal{K}^\top\mathbb{G}^\top\mathbb{M}^1$ for a shorter notation, we solve this again with the Crank-Nicolson method:

$$\boldsymbol{\rho}^{n+1} = \boldsymbol{\rho}^n - \frac{\Delta t}{2}\mathbb{D}\mathcal{Q}(\mathbf{u}^{n+1} + \mathbf{u}^n), \tag{4.20}$$

$$\begin{pmatrix} \mathcal{A} & \frac{\Delta t}{2}\mathbb{M}^1\mathbb{G} \\ -\frac{\Delta t}{2}\mathbb{L} & \mathbb{M}^0 \end{pmatrix}\begin{pmatrix} \mathbf{u}^{n+1} \\ \mathbf{p}^{n+1} \end{pmatrix} = \begin{pmatrix} \mathcal{A} & -\frac{\Delta t}{2}\mathbb{M}^1\mathbb{G} \\ \frac{\Delta t}{2}\mathbb{L} & \mathbb{M}^0 \end{pmatrix}\begin{pmatrix} \mathbf{u}^{n} \\ \mathbf{p}^{n} \end{pmatrix} + \begin{pmatrix} \Delta t\mathbb{M}^1\mathcal{P}\mathbf{b}^n \\ 0 \end{pmatrix}. \tag{4.21}$$

Hence, we first compute $\mathbf{u}^{n+1}$ and $\mathbf{p}^{n+1}$ from (4.21) and then $\boldsymbol{\rho}^{n+1}$ from (4.20). Note that (4.20) implies exact conservation of mass due to the same argument as in (3.12), namely that the basis functions in V_3 are all normalized to one on the logical domain $\hat{\Omega}$. Consequently, the discrete mass is just the sum of the coefficients $\boldsymbol{\rho}$ and from (4.20) it follows that

$$M_h^{n+1} = \sum_{i=0}^{N^3-1} \rho_i^{n+1} = \sum_{i=0}^{N^3-1} \rho_i^n = M_h^n, \tag{4.22}$$

due to the form of $\mathbb{D}$ containing only 1, -1 and 0. We denote the corresponding integrator by $\Phi^6_{\Delta t} : \mathbb{R}^{N^3} \times \mathbb{R}^{N^1} \times \mathbb{R}^{N^0} \to \mathbb{R}^{N^3} \times \mathbb{R}^{N^1} \times \mathbb{R}^{N^0}$, $\boldsymbol{\rho}^n, \mathbf{u}^n, \mathbf{p}^n \mapsto \boldsymbol{\rho}^{n+1}, \mathbf{u}^{n+1}, \mathbf{p}^{n+1}$.

In summary, in order to go from time step t_n to t_{n+1}, we successively apply the six integrators, where it is important to note that the input of the next integrator must be the output of the previous integrator:

$$\Phi_{\Delta t} := \Phi^6_{\Delta t} \circ \Phi^5_{\Delta t} \circ \Phi^4_{\Delta t} \circ \Phi^3_{\Delta t} \circ \Phi^2_{\Delta t} \circ \Phi^1_{\Delta t}. \tag{4.23}$$

This first-order compositions is also know as the Lie-Trotter splitting []. We remark, however, that higher-order compositions are available and can be found e.g. in [23].´

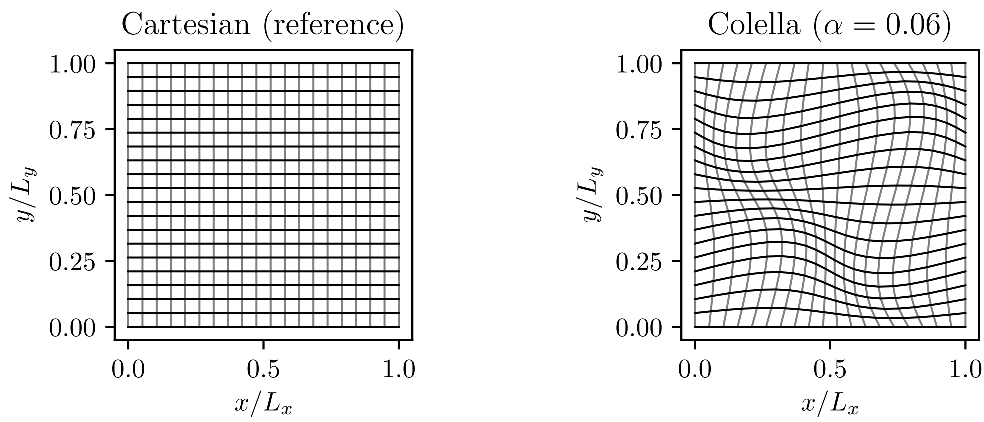

Figure 3: Exemplary meshes in the $xy-$ plane corresponding to the two mappings defined in (5.1). For the Colella mapping (right) the parameter $\alpha = 0.06$.

5 Numerical experiments

In this section we present a collection of numerical results obtained with the techniques shown in the previous sections. Here, we shall use only two types of mappings, where the first one is a standard Cartesian mapping $\boldsymbol{F}_{\mathrm{Ca}}$ which we we use as a reference and the second one a so-called Colella mapping $\boldsymbol{F}_{\mathrm{Co}}$ with which we test the impact of a distortion of the finite element mesh:

$$\boldsymbol{F}_{\mathrm{Ca}} : \hat{\Omega} \to \Omega, \boldsymbol{\eta} \mapsto \begin{pmatrix} L_x\eta_1 \\ L_y\eta_2 \\ L_z\eta_3 \end{pmatrix} = \boldsymbol{x}, \quad \boldsymbol{F}_{\mathrm{Co}} : \hat{\Omega} \to \Omega, \boldsymbol{\eta} \mapsto \begin{pmatrix} L_x(\eta_1 + \alpha\sin(2\pi\eta_1)\sin(2\pi\eta_2)) \\ L_y(\eta_2 + \alpha\sin(2\pi\eta_2)\sin(2\pi\eta_3)) \\ L_z\eta_3 \end{pmatrix} = \boldsymbol{x}. \quad (5.1)$$

Here, $L_x, L_y, L_z > 0$ are the side lengths of the rectangular physical domain Ω and $0 \leq \alpha < 1/(2\pi)$ is a parameter describing the distortion of the mesh. The upper limit for α is chosen such that the mapping does not becomes singular anywhere in the domain Ω. Note that all quantities related to the mapping, such as the Jacobian determinant or the metric tensor, are constant and diagonal in case of the Cartesian mapping. Both is not true anymore in case of the Colella mapping. Figure 3 displays the resulting coordinate lines in the xy-plane and we note that the Colella mapping collapses to the Cartesian mapping for $\alpha = 0$.

Furthermore, in all simulations shown, we assume a uniform equilibrium bulk plasma in physical space[7]. The first two subsections focus on linear MHD waves and linear wave-particle interactions. In contrast to that, the third subsection focuses on longer simulations deep into the nonlinear phase.

5.1 Pure MHD

In this paragraph we set the contribution from the kinetic ions to zero ($f_{\mathrm{h}} = 0$ for all times) and investigate linear MHD waves within the framework of STRUPHY. The dispersion relation for waves propagating in the x-direction ($\boldsymbol{k} = k\boldsymbol{e}_x$) in a homogeneous plasma of pressure p_{eq} and density ρ_{eq} in a magnetic field $\boldsymbol{B}_{\mathrm{eq}} = B_{0x}\boldsymbol{e}_x + B_{0y}\boldsymbol{e}_y$ reads

$$\left(\omega^2 - k^2 v_{\mathrm{A}}^2 \frac{B_{0x}^2}{B_{0x}^2 + B_{0y}^2}\right)\left[\omega^2 - \frac{1}{2}k^2(c_{\mathrm{S}}^2 + v_{\mathrm{A}}^2)(1 \pm \sqrt{1-\delta})\right] = 0, \quad \delta = \frac{4B_{0x}^2 c_{\mathrm{S}}^2 v_{\mathrm{A}}^2}{(c_{\mathrm{S}}^2 + v_{\mathrm{A}}^2)^2(B_{0x}^2 + B_{0y}^2)}, \quad (5.2)$$

where the first term in the rounds brackets represents the shear Alfvén wave and the second term in the square brackets the slow (-) and fast (+) magnetosonic wave, respectively. The two characteristic velocities are the Alfvén velocity $v_{\mathrm{A}}^2 = (B_{0x}^2 + B_{0y}^2)/(\mu_0\rho_{\mathrm{eq}})$ and the speed of sound $c_{\mathrm{S}}^2 = \gamma p_{\mathrm{eq}}/\rho_{\mathrm{eq}}$.

[7]Note that in case of the Colella mapping this is not true for the components of the corresponding differential forms on the logical domain.

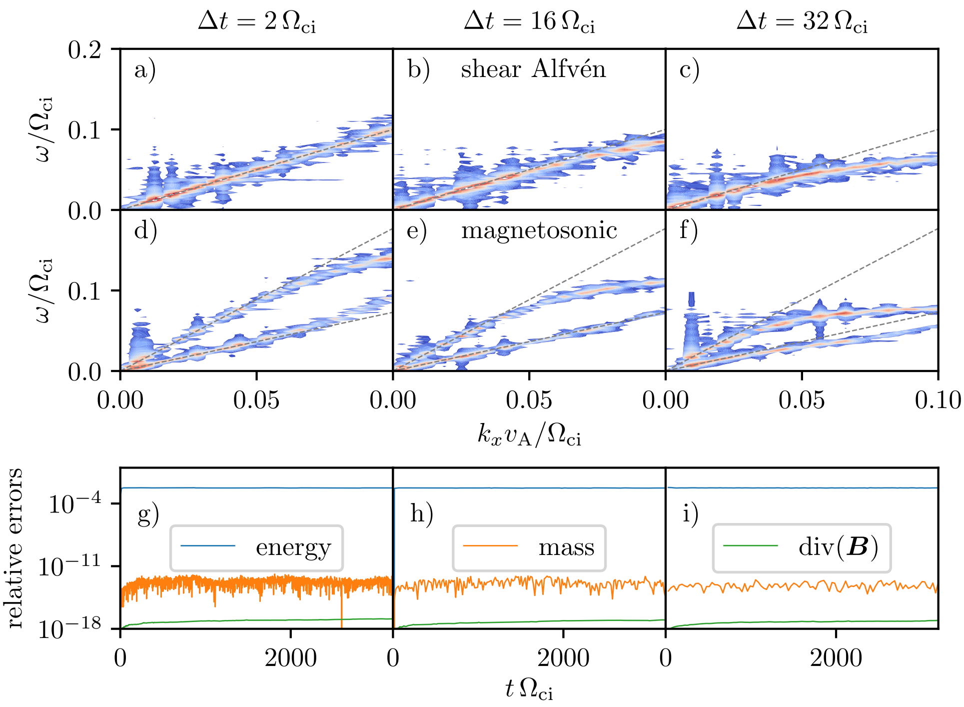

Figure 4: Normalized MHD power spectra in the $\omega - k_x$-plane for different time steps obtained by initialization with white noise. Parameters are $N_{el} = (128, 16, 2)$, $p = (2, 2, 1)$, $L_x = 3200\, v_A/\Omega_{ci}$, $L_y = 40\, v_A/\Omega_{ci}$, $L_z = 5\, v_A/\Omega_{ci}$, periodic boundary conditions everywhere, $n_{q,el} = (3, 3, 2)$ and $n_{pr,el} = (3, 3, 2)$. Top: U_z-spectra (shear Alfvén waves), bottom: p-spectra (magnetosonic waves).

To compare simulated waves to the analytical dispersion relation, we initalize STRUPHY with random noise in x-direction, meaning that we do not compute the initial finite element coefficients from some prescribed initial condition, but we load the finite element coefficients randomly in physical x-direction. Moreover, we set $\beta = 2\mu_0 p_{eq}/(B_{0x}^2 + B_{0y}^2) = 1$ and $B_{0x} = B_{0y}$ which results in $c_S = \sqrt{\gamma/2}\, v_A$. We normalize frequencies to the ion cyclotron frequency Ω_{ci} and velocities to the Alfvén velocity. This results in a normalization of spatial scales to v_A/Ω_{ci}.

We perform to tests: First, we increase the time step Δt time integration scheme for the Cartesian mapping and second, we increase the parameter α for a fixed time step in order to check the impact of the mapping on the MHD spectra. Figure 4 shows the resulting spectra for times steps $\Delta t = 4\,\Omega_{ci}$, $\Delta t = 16\,\Omega_{ci}$ and $\Delta t = 32\,\Omega_{ci}$.

5.2 Wave-particle resonance

In this section, we include an additional species of kinetic ions with an initial ($t = 0$) isotropic, shifted Maxwellian distribution function of the form

$$f_h(\boldsymbol{x}, \boldsymbol{v}, t = 0) = \frac{n_h}{\pi^{3/2} v_{th}^{3/2}} \exp\left(-\frac{(v_x - v_0)^2 + v_y^2 + v_z^2}{v_{th}^2} \right). \tag{5.3}$$

If we choose a uniform magnetic field in x-direction $\boldsymbol{B}_{eq} = B_0 \boldsymbol{e}_x$, it is straightforward to show that this distribution function is a valid choice for an equilibrium since the current carried by the hot ions also points in x-direction and hence $\boldsymbol{J}_{h,eq} \times \boldsymbol{B}_{eq} = 0$. For parallel wave propagation $\boldsymbol{k} = k\boldsymbol{e}_x$, the fully linearized system exhibits the following dispersion relation:

$$D_{R/L}(k, \omega) = \omega^2 - v_A^2 k^2 \pm \nu_h \omega \Omega_{ci} + \nu_h \Omega_{ci}^2 \frac{\omega - k v_0}{k v_{th}} Z\left(\frac{\omega - k v_0 \pm \Omega_{ci}}{k v_{th}} \right), \tag{5.4}$$

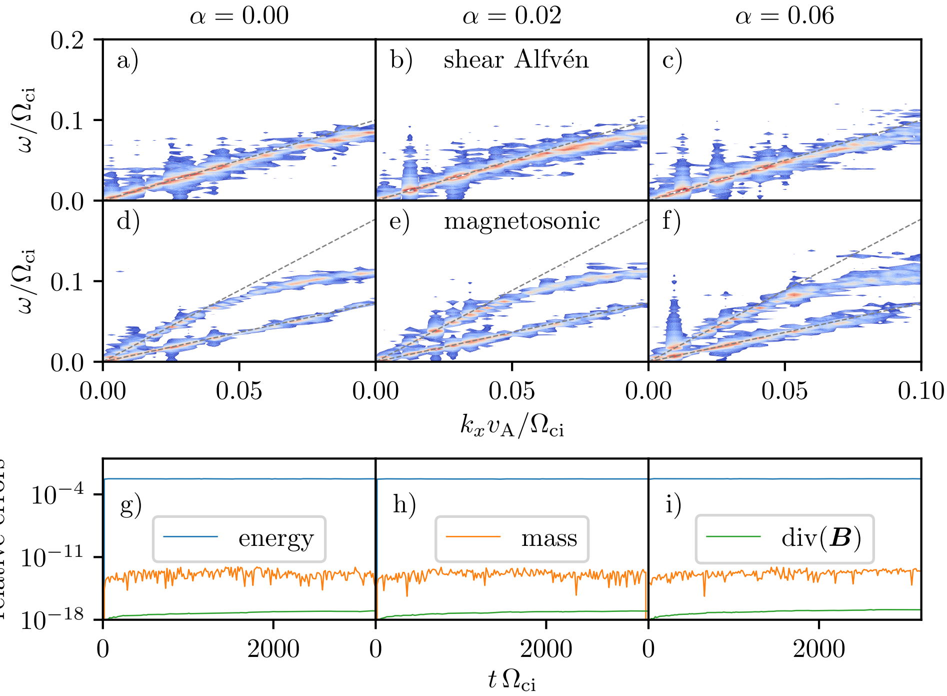

Figure 5: Normalized MHD power spectra in the $\omega - k_x$-plane for different time steps obtained by initialization with white noise. Parameters are $N_{\mathrm{el}} = (128, 16, 2)$, $p = (2, 2, 1)$, $L_x = 3200\, v_{\mathrm{A}}/\Omega_{\mathrm{ci}}$, $L_y = 40\, v_{\mathrm{A}}/\Omega_{\mathrm{ci}}$, $L_z = 5\, v_{\mathrm{A}}/\Omega_{\mathrm{ci}}$, periodic boundary conditions everywhere, $n_{\mathrm{q,el}} = (3, 3, 2)$ and $n_{\mathrm{pr,el}} = (3, 3, 2)$. Top: U_z-spectra (shear Alfvén waves), bottom: p-spectra (magnetosonic waves).

where $\nu_{\mathrm{h}} = n_{\mathrm{h}} m_{\mathrm{i}}/\rho_{\mathrm{eq}}$ is the ratio of the equilibrium bulk and energetic ion number densities, $\Omega_{\mathrm{ci}} = eB_0/m_{\mathrm{i}}$ the ion cyclotron frequency and Z denotes the plasma dispersion function

$$Z(\xi) = \sqrt{\pi}\mathrm{e}^{-\xi^2}\left(i - \frac{2}{\sqrt{\pi}}\int_0^{\xi} \mathrm{e}^{t^2}\mathrm{d}t\right) = \sqrt{\pi}\mathrm{e}^{-\xi^2}(i - \mathrm{erfi}(\xi)). \tag{5.5}$$

Note that in the absence of energetic ions ($\nu_{\mathrm{h}} = 0$) the dispersion relation coincides with the dispersion relation of shear Alvén waves. Numerically solving the dispersion relation with parameters $k = 0.8\,\Omega_{ci}/v_{\mathrm{A}}$, $v_{\mathrm{th}} = v_{\mathrm{A}}$, $v_0 = 2.5\,v_{\mathrm{A}}$ and $\nu_{\mathrm{h}} = 0.05$ yields for the R-wave an expected real frequency $\omega_{\mathrm{r}} \approx 0.8012\,\Omega_{\mathrm{ci}}$ and a growth rate (imaginary part) $\omega_{\mathrm{i}} \approx 0.0681\,\Omega_{\mathrm{ci}}$. The choice made for k is purely for testing purposes since $kv_{\mathrm{A}}/\Omega_{ci} \ll 1$ does not not result in an unstable mode in slab geometry. To excite the instability for a single wave number, we set $\boldsymbol{B}(\boldsymbol{x}, t = 0) = 10^{-3}\sin(kx)\boldsymbol{e}_z$ which corresponds to the excitation of a shear Alfvén wave. The amplitude is chosen such that it is not too small to reach the particle noise level, and not to high to start with nonlinear terms. Numerical parameters which we fix, is the number of elements $N_{\mathrm{el}} = (16, 16, 2)$, the B-spline degrees $p = (2, 2, 1)$, the number of quadrature points per element (for the computation of mass matrices) $n_{\mathrm{q,el}} = (6, 6, 2)$, the number of quadrature points per integration interval of histopolations $n_{\mathrm{q,pr}} = (6, 6, 2)$ and the size of the physical domain $L = (2\pi/0.8, 2\pi/0.8, 1)$. Furthermore, we load particles uniformly random in the logical domain and normally random in velocity space (including the shift in v_x-direction), such that the initial sampling density and particle weights

$$\bar{s}^0_{\mathrm{h}}(\boldsymbol{\eta}, \boldsymbol{v}) = \frac{1}{\pi^{3/2} v_{\mathrm{th}}^{3/2}} \exp\left(-\frac{(v_x - v_0)^2 + v_y^2 + v_z^2}{v_{\mathrm{th}}^2}\right) \Rightarrow w_k = \frac{\hat{f}^0_{\mathrm{h}}(\boldsymbol{\eta}^0_k, \boldsymbol{v}^0_k)\sqrt{g}(\boldsymbol{\eta}^0_k)}{N_{\mathrm{p}}\bar{s}^0_{\mathrm{h}}(\boldsymbol{\eta}^0_k, \boldsymbol{v}^0_k)} = \frac{n_{\mathrm{h}}\sqrt{g}(\boldsymbol{\eta}^0_k)}{N_{\mathrm{p}}}. \tag{5.6}$$

Therefore, the particle weights are all the same in case of the Cartesian mapping but not in case of the Colella mapping with $\alpha \neq 0$ due to the Jacobian determinant $\sqrt{g}$.

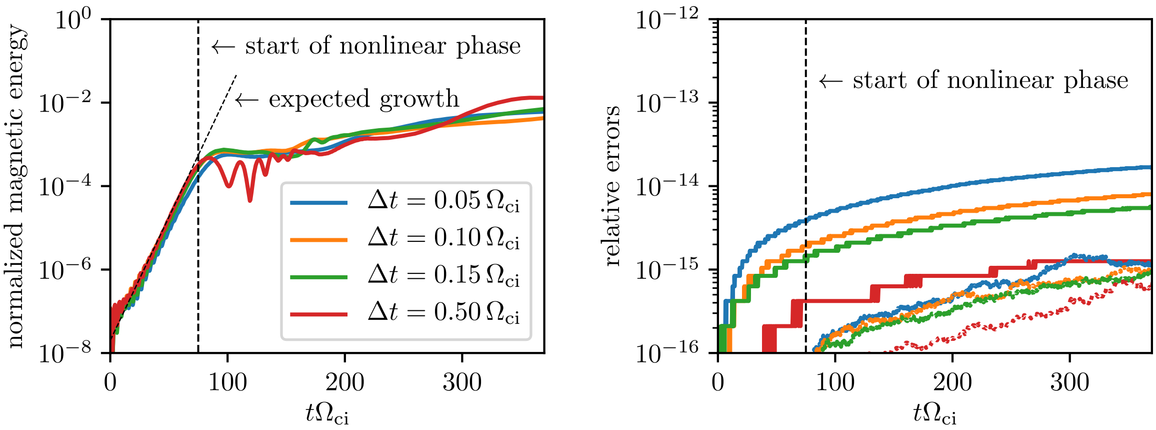

Figure 6: Normalized MHD power spectra in the $\omega - k_x$-plane for different time steps obtained by initialization with white noise. Parameters are $N_{\mathrm{el}} = (128, 16, 2)$, $p = (2, 2, 1)$, $L_x = 3200\, v_{\mathrm{A}}/\Omega_{\mathrm{ci}}$, $L_y = 40\, v_{\mathrm{A}}/\Omega_{\mathrm{ci}}$, $L_z = 5\, v_{\mathrm{A}}/\Omega_{\mathrm{ci}}$, periodic boundary conditions everywhere, $n_{\mathrm{q,el}} = (3, 3, 2)$ and $n_{\mathrm{pr,el}} = (3, 3, 2)$. Top: U_z-spectra (shear Alfvén waves), bottom: p-spectra (magnetosonic waves).

6 Summary

We presented a new hybrid kinetic MHD-kinetic code which solves linearized, ideal magnetohydrodynamics, coupled nonlinearly to fully kinetic 6d Vlasov equations. For this, we first derived the appropriate model equations by means of differential forms, valid in arbitrary Riemannian metric, in order to apply the framework of finite element exterior calculus for the spatial discretization. Choosing compatible finite element spaces and projectors onto them satisfying a commuting diagram with an exact de Rham sequence and applying classical particle-in-cell techniques for the Vlasov equation, we ended up with a system of equations in time with the following properties:

1. exact conservation of mass
2. exact conservation of the zero-divergence constraint $\nabla \cdot \boldsymbol{B} = 0$
3. exact conservation of energy for the energy corresponding to shear Alfvén waves

To translate the energy conservation property to the fully discrete level, we first split apart the non-Hamiltonian terms followed by Poisson splitting of the Hamiltonian part and solving each sub-step in an energy-conserving way. By performing numerical experiment for various parameters and two kind of coordinate transformation, we showed that the energy conservation properties indeed hold and that we can reproduce analytical dispersion relations for linear simulations.

Appendix A Formulae for exterior calculus of differential forms

A.1 Exterior product

The exterior (or wedge) product $a^p \wedge b^q$ relates a p-form and a q-form to a $(p+q)$-form. In terms of the components $\hat{a}^p$ (respectively $\hat{\boldsymbol{a}}^p$) and $\hat{b}^q$ ($\hat{\boldsymbol{b}}^q$), it is given by

$$\wedge : \Lambda^p(\Omega) \times \Lambda^q(\Omega) \to \Lambda^{p+q}(\Omega), \qquad \begin{cases} \hat{a}^0, \hat{\boldsymbol{b}}^q \mapsto \hat{a}^0 \hat{\boldsymbol{b}}^q, & p = 0,\ q \in \{0,1,2,3\}, \\ \hat{\boldsymbol{a}}^1, \hat{\boldsymbol{b}}^1 \mapsto \hat{\boldsymbol{a}}^1 \times \hat{\boldsymbol{b}}^1 & p = 1,\ q = 1, \\ \hat{\boldsymbol{a}}^1, \hat{\boldsymbol{b}}^2 \mapsto (\hat{\boldsymbol{a}}^1)^\top \hat{\boldsymbol{b}}^2, & p = 1,\ q = 2, \\ \hat{a}^3, \hat{\boldsymbol{b}}^q \mapsto 0, & p = 3,\ q \in \{0,1,2,3\}, \end{cases} \tag{A.1}$$

which are all possible cases due to the anti-symmetry $a^p \wedge b^q = (-1)^{pq} b^q \wedge a^p$.

A.2 Interior product

The interior product $i_{\mathsf{a}} a^p$ relates a vector field a and a p-form a^p to a $(p-1)$-form. In terms of the components $\hat{\boldsymbol{a}}$ and $\hat{a}^p$ ($\hat{\boldsymbol{a}}^p$), it is given by

$$i_{\mathsf{a}} : \Lambda^p(\Omega) \times T\Omega \to \Lambda^{p-1}(\Omega), \qquad \begin{cases} \hat{a}^0 \mapsto 0, & p = 0, \\ \hat{\boldsymbol{a}}^1 \mapsto (\hat{\boldsymbol{a}}^1)^\top \hat{\boldsymbol{a}}, & p = 1, \\ \hat{\boldsymbol{a}}^2 \mapsto \hat{\boldsymbol{a}}^2 \times \hat{\boldsymbol{a}}, & p = 2, \\ \hat{a}^3 \mapsto \hat{a}^3 \hat{\boldsymbol{a}}, & p = 3. \end{cases} \tag{A.2}$$

A.3 Hodge-star operator

The Hodge-star operator $*a^p$ relates a p-form a^p to a $(3-p)$-form. In terms of the components $\hat{\boldsymbol{a}}^p$, it is given by

$$* : \Lambda^p(\Omega) \to \Lambda^{3-p}(\Omega), \qquad \begin{cases} \hat{a}^0 \mapsto \sqrt{g}\, \hat{a}^0, & p = 0, \\ \hat{\boldsymbol{a}}^1 \mapsto \sqrt{g}\, G^{-1} \hat{\boldsymbol{a}}^1, & p = 1, \\ \hat{\boldsymbol{a}}^2 \mapsto \dfrac{1}{\sqrt{g}} G \hat{\boldsymbol{a}}^2, & p = 2, \\ \hat{a}^3 \mapsto \dfrac{1}{\sqrt{g}} \hat{a}^3, & p = 3. \end{cases} \tag{A.3}$$

A.4 Exterior derivative

The exterior derivative $\mathrm{d}a^p$ acts on the components of p-forms $\hat{\boldsymbol{a}}^p$ as the grad, div and curl on scalar fields and components of vector fields in Cartesian coordinates (see Table 2).

$\mathrm{d} : \Lambda^p(\Omega) \to \Lambda^{p+1}(\Omega)$	$p = 0$	$p = 1$	$p = 2$	$p = 3$
	$\hat{a}^0 \mapsto \hat{\nabla} \hat{a}^0$	$\hat{\boldsymbol{a}}^1 \mapsto \hat{\nabla} \times \hat{\boldsymbol{a}}^1$	$\hat{\boldsymbol{a}}^2 \mapsto \hat{\nabla} \cdot \hat{\boldsymbol{a}}^2$	$\hat{a}^3 \mapsto 0$

Table 2: Exterior derivative in terms of the components $\hat{\boldsymbol{a}}^p$.

Moreover, the exterior derivative satisfies

$$1) \quad \mathrm{d}(a^p + b^p) = \mathrm{d}a^p + \mathrm{d}b^p, \tag{A.4a}$$

$$2) \quad \mathrm{d}(a^p \wedge b^q) = \mathrm{d}a^p \wedge b^q + (-1)^p a^p \wedge \mathrm{d}b^q \qquad \text{(Leibniz rule)}, \tag{A.4b}$$

$$3) \quad \mathrm{d}\mathrm{d}a^p = 0. \tag{A.4c}$$

A.5 Hilbert spaces of p-forms

The Hilbert spaces of p-forms are defined as

$$
\begin{aligned}
L^2\Lambda^p(\Omega) &:= \{a^p \in \Lambda^p(\Omega) : (a^p, a^p) < \infty\}, && \text{(A.5a)}\\
H\Lambda^p(\Omega) &:= \{a^p \in L^2\Lambda^p(\Omega),\, \mathrm{d}a^p \in L^2\Lambda^{p+1}(\Omega)\}, && \text{(A.5b)}
\end{aligned}
$$

and equipped with the following scalar product (or L^2-inner product):

$$
(\cdot,\cdot) : \Lambda^p(\Omega) \times \Lambda^p(\Omega) \to \mathbb{R}, \quad (a^p, b^p) := \int_\Omega a^p \wedge *b^p = \begin{cases} \int_{\hat\Omega} \hat a^0 \hat b^0 \sqrt{g}\, \mathrm{d}^3\eta, & p = 0,\\ \int_{\hat\Omega} (\hat{\boldsymbol{a}}^1)^\top G^{-1} \hat{\boldsymbol{b}}^1 \sqrt{g}\, \mathrm{d}^3\eta, & p = 1,\\ \int_{\hat\Omega} (\hat{\boldsymbol{a}}^2)^\top G \hat{\boldsymbol{b}}^2 \frac{1}{\sqrt{g}}\, \mathrm{d}^3\eta, & p = 2,\\ \int_{\hat\Omega} \hat a^3 \hat b^3 \frac{1}{\sqrt{g}}\, \mathrm{d}^3\eta, & p = 3. \end{cases} \tag{A.6}
$$

Note the symmetry $(a^p, b^p) = (b^p, a^p)$ of the scalar product. Due to the property (A.4c) of the exterior derivative, the Hilbert spaces of p-forms form the following chain complex

$$
H\Lambda^0(\Omega) \xrightarrow{\mathrm{d}} H\Lambda^1(\Omega) \xrightarrow{\mathrm{d}} H\Lambda^2(\Omega) \xrightarrow{\mathrm{d}} L^2\Lambda^3(\Omega), \tag{A.7}
$$

with the property that the image of the previous operator is in the kernel of the next operator.

A.6 Co-differential operator

Using generalized Stokes' theorem

$$
\int_\Omega \mathrm{d}a^p = \int_{\partial\Omega} a^p, \tag{A.8}
$$

together with Leibniz rule (A.4b) and $** = id$, we can derive the formal adjoint of the exterior derivative via

$$
\begin{aligned}
(\mathrm{d}a^{p-1}, b^p) &= \int_\Omega \mathrm{d}a^{p-1} \wedge *b^p = \int_\Omega \mathrm{d}(a^{p-1} \wedge *b^p) - (-1)^{p-1} \int_\Omega a^{p-1} \wedge \mathrm{d}(*b^p)\\
&= \int_{\partial\Omega} a^{p-1} \wedge *b^p + (-1)^p \int_\Omega a^{p-1} \wedge **\,\mathrm{d}(*b^p)\\
&= \int_{\partial\Omega} a^{p-1} \wedge *b^p + (-1)^p (a^{p-1}, *\mathrm{d}*b^p).
\end{aligned} \tag{A.9}
$$

The operator

$$
\mathrm{d}^* : \Lambda^p_{\boldsymbol{x}}(\Omega) \to \Lambda^{p-1}_{\boldsymbol{x}}(\Omega), \qquad a^p \mapsto \mathrm{d}^* a^p = (-1)^p * \mathrm{d} * a^p, \tag{A.10}
$$

is called the *co-differential* operator.

Appendix B δf-method

The δf-method is a common approach for noise reduction in PIC codes. The main assumption is that the unknown distribution function f_h remains close to some known distribution function, which, typically but not necessarily, is the equilibrium distribution function $f_{\mathrm{h,eq}}$ for which (ideally) analytical moments in velocity space

$$
\rho_{\mathrm{ch,eq}} = q_\mathrm{h} \int_{\mathbb{R}^3} f_{\mathrm{h,eq}}\, \mathrm{d}^3v, \qquad \boldsymbol{J}_{\mathrm{h,eq}} = q_\mathrm{h} \int_{\mathbb{R}^3} \boldsymbol{v} f_{\mathrm{h,eq}}\, \mathrm{d}^3v, \tag{B.1}
$$

are available. Therefore, only the perturbed part of the distribution function is integrated using the particles. Using $f_\mathrm{h} = (f_\mathrm{h} - f_\mathrm{h,eq}) + f_\mathrm{h,eq}$, we modify (3.71)-(3.73) in the following way:

$$\mathrm{CC}(\rho_\mathrm{ch}) \approx \int_{\hat\Omega}\int_{\mathbb{R}^3} \left\{ \hat{\boldsymbol{C}}_h^\top G^{-1} \frac{\hat f_\mathrm{h} - \hat f_\mathrm{h,eq}}{\hat s_\mathrm{h}} \left(\hat{\boldsymbol{B}}^2_{\mathrm{f}h} \times G^{-1}\hat{\boldsymbol{U}}^1_h \right) \right\} \hat s_\mathrm{h} \sqrt{g}\, \mathrm{d}^3 v\, \mathrm{d}^3\eta \tag{B.2}$$

$$+ \int_{\hat\Omega} (\hat{\boldsymbol{C}}^1_h)^\top G^{-1} \hat\rho_\mathrm{ch,eq} \left(\hat{\boldsymbol{B}}^2_{\mathrm{f}h} \times G^{-1}\hat{\boldsymbol{U}}^1_h \right) \sqrt{g}\, \mathrm{d}^3\eta \tag{B.3}$$

$$\approx \sum_{k=1}^K \underbrace{\frac{1}{K} \left(\frac{\hat f^0_\mathrm{h}(\boldsymbol{\eta}^0_k, \boldsymbol{v}^0_k)}{\hat s^0_\mathrm{h}(\boldsymbol{\eta}^0_k, \boldsymbol{v}^0_k)} - \frac{\hat f_\mathrm{h,eq}(\boldsymbol{\eta}_k, \boldsymbol{v}_k)}{\hat s^0_\mathrm{h}(\boldsymbol{\eta}^0_k, \boldsymbol{v}^0_k)} \right)}_{=:w_k(\boldsymbol{\eta}_k(t), \boldsymbol{v}_k(t))} (\hat{\boldsymbol{C}}^1_h)^\top(\boldsymbol{\eta}_k) G^{-1}(\boldsymbol{\eta}_k) \left(\hat{\boldsymbol{B}}^2_{\mathrm{f}h}(\boldsymbol{\eta}_k) \times G^{-1}(\boldsymbol{\eta}_k) \hat{\boldsymbol{U}}^1_h(\boldsymbol{\eta}_k) \right) \tag{B.4}$$

$$+ \mathbf{c}^\top \int_{\hat\Omega} \mathbb{A}^1 \frac{\hat\rho_\mathrm{ch,eq}}{\sqrt{g}} \mathbb{B}^G (\mathbb{A}^1)^\top \, \mathrm{d}^3\eta\, \mathbf{u} = \mathbf{c}^\top \mathbb{P}^1 \mathbb{W} \bar G^{-1} \mathbb{B}_\mathrm{f} \bar G^{-1} (\mathbb{P}^1)^\top \mathbf{u} + \mathbf{c}^\top \mathbb{X}^1(\mathbf{b}) \mathbf{u}. \tag{B.5}$$

Hence we get two modifications compared to the full-f description: First, the particle weights are not constant anymore but depend on the particle positions in phase space. Second, we get an additional term with the weighted mass matrix $\mathbb{X}^1(\mathbf{b})$, where $\mathbb{B}^G$ denotes once more the cross-product in terms of a matrix-vector product as in (3.16) but built from the three components of $G\hat{\boldsymbol{B}}^2_\mathrm{fh} = G(\hat{\boldsymbol{B}}^2_\mathrm{eq} + \mathbf{b}^\top \mathbb{A}^2)$. Straightforwardly, we obtain in the same way for the term involving the current density

$$\mathrm{CC}(\boldsymbol{J}_\mathrm{h}) \approx \mathbf{c}^\top \mathbb{P}^1 \mathbb{W} \bar G^{-1} \mathbb{B}_\mathrm{f} \bar{DF}^{-1} \boldsymbol{V} + \mathbf{c}^\top \int_{\hat\Omega} \mathbb{A}^1 \frac{1}{\sqrt{g}} \left((G\hat{\boldsymbol{B}}^2_{\mathrm{f}h}) \times (G\hat{\boldsymbol{J}}_\mathrm{h,eq}) \right) \mathrm{d}^3\eta \tag{B.6}$$

$$= \mathbf{c}^\top \mathbb{P}^1 \mathbb{W} \bar G^{-1} \mathbb{B}_\mathrm{f} \bar{DF}^{-1} \boldsymbol{V} + \mathbf{c}^\top \mathbf{x}(\mathbf{b}), \tag{B.7}$$

where it is important to note that $\hat{\boldsymbol{J}}_\mathrm{h,eq}$ are the components of the vector field corresponding to the equilibrium current density. Regarding the time stepping scheme, we simply add the new terms in sub-steps 1 and 3, respectively, and solve in the same way for $\mathbf{u}^{n+1}$ (sub-step 1) and $\mathbf{u}^{n+1}, \boldsymbol{V}^{n+1}$ (sub-step 3) as before using the Crank-Nicolson method. Moreover, we assume the weights to be constant in sub-step 3. In the end of a time step we then update the weights according to (B.4). However, this method breaks the energy conservation property of the Hamiltonian part, since we loose the anti-symmetry of the Poisson matrix.

Appendix C Weights in quasi spline interpolation

	ω^i $(p=2)$		ω^i $(p=3)$	
clamped			$\{1,0,0,0,0\}$,	$i=0$
	$\{1,0,0\}$,	$i=0$	$\{-\frac{5}{18}, \frac{40}{18}, -\frac{24}{18}, \frac{8}{18}, -\frac{1}{18}\}$,	$i=1$
	$\{-\frac{1}{2}, 2, -\frac{1}{2}\}$,	$0<i<\hat n_N-1$	$\{\frac{1}{6}, -\frac{8}{6}, \frac{20}{6}, -\frac{8}{6}, \frac{1}{6}\}$,	$1<i<\hat n_N-2$
	$\{0,0,1\}$,	$i=\hat n_N-1$	$\{-\frac{1}{18}, \frac{8}{18}, -\frac{24}{18}, \frac{40}{18}, -\frac{5}{18}\}$,	$i=\hat n_N-2$
			$\{0,0,0,0,1\}$,	$i=\hat n_N-1$
periodic	$\{-\frac{1}{2}, 2, -\frac{1}{2}\}$,	$\forall\, i$	$\{\frac{1}{6}, -\frac{8}{6}, \frac{20}{6}, -\frac{8}{6}, \frac{1}{6}\}$,	$\forall\, i$

Table 3: The weights in (3.58) for the interpolator I^p for quadratic $(p=2)$ and cubic $(p=3)$ B-splines, respectively.

	$\tilde{\omega}^i$ $(p=2)$		$\tilde{\omega}^i$ $(p=3)$	
clamped			$\{\frac{23}{18}, -\frac{17}{18}, \frac{7}{18}, -\frac{1}{18}, 0, 0\}$,	$i=0$
	$\{\frac{3}{2}, -\frac{1}{2}, 0\}$,	$i=0$	$\{-\frac{8}{18}, \frac{56}{18}, -\frac{28}{18}, \frac{4}{18}, 0, 0\}$,	$i=1$
	$\{-\frac{1}{2}, \frac{3}{2}, \frac{3}{2}, -\frac{1}{2}\}$,	$0<i<\hat{n}_D-1$	$\{\frac{3}{18}, -\frac{21}{18}, \frac{36}{18}, \frac{36}{18}, -\frac{21}{18}, \frac{3}{18}\}$,	$1<i<\hat{n}_D-2$
	$\{0, -\frac{1}{2}, \frac{3}{2}\}$,	$i=\hat{n}_D-1$	$\{0, 0, \frac{4}{18}, -\frac{28}{18}, \frac{56}{18}, -\frac{8}{18}\}$,	$i=\hat{n}_D-2$
			$\{0, 0, -\frac{1}{18}, \frac{7}{18}, -\frac{17}{18}, \frac{23}{18}\}$,	$i=\hat{n}_D-1$
periodic	$\{-\frac{1}{2}, \frac{3}{2}, \frac{3}{2}, -\frac{1}{2}\}$,	$\forall\, i$	$\{\frac{3}{18}, -\frac{21}{18}, \frac{36}{18}, \frac{36}{18}, -\frac{21}{18}, \frac{3}{18}\}$,	$\forall\, i$

Table 4: The weights in (3.62) for the histopolator H^{p-1} for quadratic ($p=2$) and cubic ($p=3$) B-splines, respectively.

References

[1] D. Arnold, R. Falk, and R. Winther. Finite element exterior calculus: from Hodge theory to numerical stability. *Bulletin of the American mathematical society*, 47(2):281–354, 2010.

[2] D. N. Arnold. *Finite element exterior calculus*, volume 93. SIAM, 2018.

[3] D. N. Arnold, R. S. Falk, and R. Winther. Finite element exterior calculus, homological techniques, and applications. *Acta numerica*, 15:1–155, 2006.

[4] A. Y. Aydemir. A unified monte carlo interpretation of particle simulations and applications to non-neutral plasmas. *Physics of Plasmas*, 1(4):822–831, 1994.

[5] E. Belova, R. Denton, and A. Chan. Hybrid simulations of the effects of energetic particles on low-frequency MHD waves. *Journal of Computational Physics*, 136(2):324–336, 1997.

[6] S. Briguglio, G. Vlad, F. Zonca, and C. Kar. Hybrid magnetohydrodynamic-gyrokinetic simulation of toroidal Alfvén modes. *Physics of Plasmas*, 2(10):3711–3723, 1995.

[7] A. Buffa, G. Sangalli, and R. Vázquez. Isogeometric analysis in electromagnetics: B-splines approximation. *Computer Methods in Applied Mechanics and Engineering*, 199:1143–1152, 03 2010.

[8] J. W. Burby and C. Tronci. Variational approach to low-frequency kinetic-MHD in the current coupling scheme. *Plasma Physics and Controlled Fusion*, 59(4):045013, 2017.

[9] W. Burtis and R. Helliwell. Magnetospheric chorus: Occurrence patterns and normalized frequency. *Planetary and Space Science*, 24(11):1007 – 1024, 1976.

[10] G. Chen and L. Chacón. An energy-and charge-conserving, nonlinearly implicit, electromagnetic 1D-3V Vlasov–Darwin particle-in-cell algorithm. *Computer Physics Communications*, 185(10):2391–2402, 2014.

[11] L. Chen and F. Zonca. Physics of Alfvén waves and energetic particles in burning plasmas. *Reviews of Modern Physics*, 88(1):015008, 2016.

[12] J. Crank and P. Nicolson. A practical method for numerical evaluation of solutions of partial differential equations of the heat-conduction type. *Mathematical Proceedings of the Cambridge Philosophical Society*, 43(1):50–67, 1947.

[13] C. de Boor and G. Fix. Spline approximation by quasiinterpolants. *Journal of Approximation Theory*, 8(1):19 – 45, 1973.

[14] E. Evstatiev and B. Shadwick. Variational formulation of particle algorithms for kinetic plasma simulations. *Journal of Computational Physics*, 245:376–398, 2013.

[15] G. Farin. *Curves and Surfaces for Computer-Aided Geometric Design*. Academic Press, 1993.

[16] T. Frankel. *The Geometry of Physics: An Introduction*. Cambridge University Press, 3 edition, 2011.

[17] Y. He, H. Qin, Y. Sun, J. Xiao, R. Zhang, and J. Liu. Hamiltonian time integrators for Vlasov-Maxwell equations. *Physics of Plasmas*, 22(12):124503, 2015.

[18] Y. He, Y. Sun, H. Qin, and J. Liu. Hamiltonian particle-in-cell methods for Vlasov-Maxwell equations. *Physics of Plasmas*, 23(9):092108, 2016.

[19] W. Heidbrink. Basic physics of Alfvén instabilities driven by energetic particles in toroidally confined plasmas. *Physics of Plasmas*, 15(5):055501, 2008.

[20] A. Könies, S. Briguglio, N. Gorelenkov, T. Fehér, M. Isaev, P. Lauber, A. Mishchenko, D. Spong, Y. Todo, W. Cooper, et al. Benchmark of gyrokinetic, kinetic MHD and gyrofluid codes for the linear calculation of fast particle driven TAE dynamics. *Nuclear Fusion*, 58(12):126027, 2018.

[21] M. Kraus, K. Kormann, P. J. Morrison, and E. Sonnendrücker. GEMPIC: Geometric electromagnetic particle-in-cell methods. *Journal of Plasma Physics*, 83(4), 2017.

[22] P. Lauber. Super-thermal particles in hot plasmas—Kinetic models, numerical solution strategies, and comparison to tokamak experiments. *Physics Reports*, 533(2):33–68, 2013.

[23] R. I. McLachlan and G. R. W. Quispel. Splitting methods. *Acta Numerica*, 11:341–434, 2002.

[24] P. J. Morrison. Structure and structure-preserving algorithms for plasma physics. *Physics of Plasmas*, 24(5):055502, 2017.

[25] P. J. Morrison and J. M. Greene. Noncanonical Hamiltonian density formulation of hydrodynamics and ideal magnetohydrodynamics. *Physical Review Letters*, 45(10):790, 1980.

[26] W. Park, E. Belova, G. Fu, X. Tang, H. Strauss, and L. Sugiyama. Plasma simulation studies using multilevel physics models. *Physics of Plasmas*, 6(5):1796–1803, 1999.

[27] H. Qin, J. Liu, J. Xiao, R. Zhang, Y. He, Y. Wang, Y. Sun, J. W. Burby, L. Ellison, and Y. Zhou. Canonical symplectic particle-in-cell method for long-term large-scale simulations of the Vlasov–Maxwell equations. *Nuclear Fusion*, 56(1):014001, 2015.

[28] O. Santolík, D. A. Gurnett, J. S. Pickett, M. Parrot, and N. Cornilleau-Wehrlin. A microscopic and nanoscopic view of storm-time chorus on 31 march 2001. *Geophysical Research Letters*, 31(2), 2004.

[29] J. Squire, H. Qin, and W. M. Tang. Geometric integration of the Vlasov-Maxwell system with a variational particle-in-cell scheme. *Physics of Plasmas*, 19(8):084501, 2012.

[30] Y. Todo and T. Sato. Linear and nonlinear particle-magnetohydrodynamic simulations of the toroidal Alfvén eigenmode. *Physics of plasmas*, 5(5):1321–1327, 1998.

[31] C. Tronci. Hamiltonian approach to hybrid plasma models. *Journal of Physics A: Mathematical and Theoretical*, 43(37):375501, 2010.

[32] B. T. Tsurutani and E. J. Smith. Postmidnight chorus: A substorm phenomenon. *Journal of Geophysical Research (1896-1977)*, 79(1):118–127, 1974.

[33] X. Wang, S. Briguglio, L. Chen, C. Di Troia, G. Fogaccia, G. Vlad, and F. Zonca. An extended hybrid magnetohydrodynamics gyrokinetic model for numerical simulation of shear Alfvén waves in burning plasmas. *Physics of Plasmas*, 18(5):052504, 2011.

[34] J. Xiao and H. Qin. Field theory and a structure-preserving geometric particle-in-cell algorithm for drift wave instability and turbulence. *Nuclear Fusion*, 59(10):106044, 2019.

[35] J. XIAO, H. QIN, and J. LIU. Structure-preserving geometric particle-in-cell methods for Vlasov-Maxwell systems. *Plasma Science and Technology*, 20(11):110501, sep 2018.

[36] J. Xiao, H. Qin, J. Liu, and R. Zhang. Local energy conservation law for a spatially-discretized Hamiltonian Vlasov-Maxwell system. *Physics of Plasmas*, 24(6):062112, 2017.